AD-A056 895 JOHNS HOPKINS UNIV LAUREL MD APPLIED PHYSICS LAB F/G 3/1
PREDICTION OF SOLAR PARTICLE EVENTS AND GEOMAGNETIC ACTIVITY US--ETC(U)
MAY 78 E C ROELOF, B L GOTWOLS, D G MITCHELL AFOSR-77-0007
UNCLASSIFIED AFOSR-TR-78-1211 NL

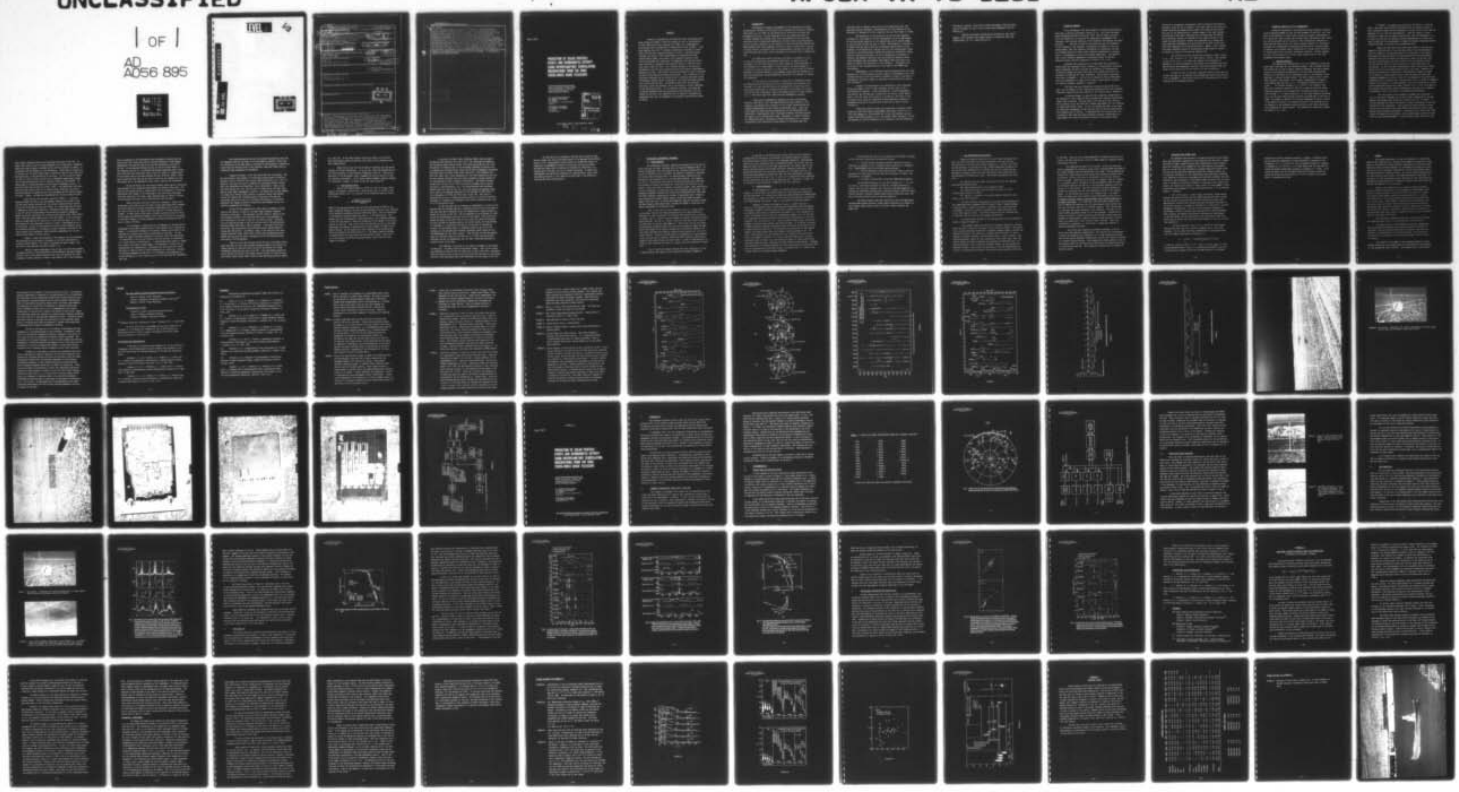

END
DATE FILMED
9-78
DDC

UNCLASSIFIED

SECURITY CLASSIFICATION OF THIS PAGE (When Data Entered)

REPORT DOCUMENTATION PAGE

READ INSTRUCTIONS BEFORE COMPLETING FORM

1. REPORT NUMBER: AFOSR-TR-78-1211	2. GOVT ACCESSION NO.
3. RECIPIENT'S CATALOG NUMBER	
4. TITLE (and Subtitle): PREDICTION OF SOLAR PARTICLE EVENTS AND GEOMAGNETIC ACTIVITY USING INTERPLANETARY SCINTILLATION OBSERVATIONS FROM THE IOWA COCOA-CROSS RADIO TELESCOPE.	5. TYPE OF REPORT & PERIOD COVERED: Final, 1 Apr 76- 31 Mar 78.
6. PERFORMING ORG. REPORT NUMBER	
7. AUTHOR(s): E. C. Roelof, B. L. Gotwols, D. G. Mitchell, W. M. Cronyn, S. D. Shawhan	8. CONTRACT OR GRANT NUMBER(s): AFOSR-77-3406
9. PERFORMING ORGANIZATION NAME AND ADDRESS: Johns Hopkins University Applied Physics Lab. Johns Hopkins Road Laurel, MD 20810	10. PROGRAM ELEMENT, PROJECT, TASK AREA & WORK UNIT NUMBERS: 2311 A1, 61102 F, A1
11. CONTROLLING OFFICE NAME AND ADDRESS: AFOSR/ NP Bolling AFB, Wash. D.C. 20332	12. REPORT DATE: May 78; NUMBER OF PAGES: 20
14. MONITORING AGENCY NAME & ADDRESS (if different from Controlling Office)	15. SECURITY CLASS. (of this report): UNCLASSIFIED
	15a. DECLASSIFICATION/DOWNGRADING SCHEDULE

16. DISTRIBUTION STATEMENT (of this Report)

Approved for public release;
distribution unlimited.

17. DISTRIBUTION STATEMENT (of the abstract entered in Block 20, if different from Report)

DDC RECEIVED AUG 1 1978 E

18. SUPPLEMENTARY NOTES

19. KEY WORDS (Continue on reverse side if necessary and identify by block number)

20. ABSTRACT (Continue on reverse side if necessary and identify by block number)

Synoptic interplanetary scintillation (IPS) observations were taken during the summer of 1976 and autumn of 1977 on the University of Iowa COCOA-Cross radio telescope (34.3 MHz), with supplementary observations from the University of Maryland TPT array (38 MHz). A new high sampling rate (10 times per second) digital system made it possible to reconstruct the IPS powerspectrum between 0.1-3.0 Hz. The observations, combined with earlier (1974) measurements of integrated IPS power (scintillation index), have lead

(con't. on reverse side)

DD FORM 1 JAN 73 1473 EDITION OF 1 NOV 65 IS OBSOLETE

UNCLASSIFIED

SECURITY CLASSIFICATION OF THIS PAGE (When Data Entered)

031 650

20. (Con't)

to the conclusion (based on theoretical modelling) that prediction of activity and associated variations in energetic solar particle events is feasible with a lead time of about 24 hours. The technique depends on the observed broadening of the IPS power spectrum as solar wind density enhancements approach the earth. This effect has been documented for both co-rotating and solar flare-associated plasma disturbances. Full validation of the prediction technique was not possible due to extensive down-time caused by unusually adverse weather conditions at the Clark Lake Radio Observatory in both 1976 and 1977. Consequently about half the available resources, fiscal and manpower, had to be devoted to a major upgrading of the COCOA-Cross array. In its improved condition, and using new techniques developed from the observational and theoretical work performed in 1976-1977, the COCOA-Cross may be capable of extending the prediction lead time for geomagnetic disturbances significantly beyond 24 hours.

May 1978

PREDICTION OF SOLAR PARTICLE EVENTS AND GEOMAGNETIC ACTIVITY USING INTERPLANETARY SCINTILLATION OBSERVATIONS FROM THE IOWA COCOA-CROSS RADIO TELESCOPE

Final Scientific Report Covering the Period 1 April 1976 – 31 March 1978, on Contract NPP-75-157, Air Force Office of Scientific Research

E. C. Roelof, Principal Investigator
B. L. Gotwols, Co-Investigator
D. G. Mitchell
Johns Hopkins University Applied Physics Laboratory

W. M. Cronyn, Co-Investigator
S. D. Shawhan, Co-Investigator
J. J. Rickard
University of Iowa

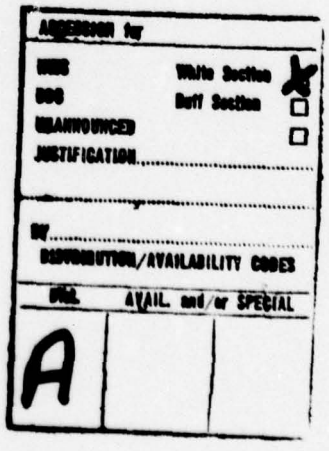

Johns Hopkins Road, Laurel, Maryland 20810

ABSTRACT

Synoptic interplanetary scintillation (IPS) observations were taken during the summer of 1976 and authumn of 1977 on the University of Iowa COCOA-Cross radio telescope (34.3 MHz), with supplementary observations from the University of Maryland TPT array (38 MHz). A new high sampling rate (10 s^{-1}) digital system made it possible to reconstruct the IPS power spectrum between 0.1-3.0 Hz. The observations, combined with earlier (1974) measurements of integrated IPS power (scintillation index), have lead to the conclusion (based on theoretical modelling) that prediction of geomagnetic activity and associated variations in energetic solar particle events is feasible with a lead time of about 24 hours. The technique depends on the observed broadening of the IPS power spectrum as solar wind density enhancements approach the earth. This effect has been documented for both co-rotating and solar flare-associated plasma disturbances. Full validation of the prediction technique was not possible due to extensive down-time caused by unusually adverse weather conditions at the Clark Lake Radio Observatory in both 1976 and 1977. Consequently about half the available resources, fiscal and manpower, had to be devoted to a major upgrading of the COCOA-Cross array. In its improved condition, and using new techniques developed from the observational and theoretical work performed in 1976-1977, the COCOA-Cross may be capable of extending the prediction lead time for geomagnetic disturbances significantly beyond 24 hours.

1. INTRODUCTION

We proposed a 24-month investigation of the feasibility of using interplanetary intensity scintillation (IPS) observations of natural celestial radio-sources at 34.3 MHz for the prediction of solar particle events and geomagnetic activity. The IPS technique is the only means available for locating, mapping and tracking large scale disturbances in the solar wind which give rise to significant geophysical activity; thus it can potentially serve to provide continuity in the hierarchy of solar-terrestrial observations which began at and in the immediate vicinity of the sun itself with a variety of radio, optical, ultraviolet and x-ray measurements, and end at or near the earth with near-earth space probe measurements and various types of geophysical data.

The COCOA-Cross Radio Telescope, with which we proposed to carry out the IPS observations, was designed specifically to exploit the IPS technique, i.e. the collecting area is large enough to allow measurement of IPS parameters on a large number of radio sources, the beam pointing is electronic to allow re-pointing to a large number of sources each day without spending an inordinate amount of time slewing (which would be required for a dish type instrument), and post-detection electronics are designed to measure IPS parameters.

At the time that we proposed to undertake the feasibility study, the COCOA-Cross had demonstrated both its operational and scientific capabilities, i.e. more than 80 sources had displayed IPS activity and daily observations extending over 6 months had revealed a succession of 13 recurrent IPS activity enhancements with a recurrence period of 27 days *(Erskine, et al., 1978)* which were well correlated with geomagnetic activity.

Other work in mathematical modeling of radio scintillation *(Mitchell and Roelof, 1976)* had demonstrated that power spectra of the intensity fluctuations were necessary for the proper interpretation and complete understanding of the intensity fluctuation data. Until this study began, the data collection capabilities of the COCOA-Cross were restricted to recording the total integrated intensity fluctuation power m^2, where m is the scintillation index. Therefore, in order to conduct the feasibility study, the group at JHU/APL (principally B. L. Gotwols) constructed a data acquisition system capable of recording high time

resolution data on magnetic tape both from the COCOA-Cross and, when observing time was available, simultaneously from both channels of the University of Maryland TPT radio telescope (also at Clark Lake) at 38 MHz.

The capability of collecting data on the TPT was originally included as a cross-check of the two instruments, and as an improvement of the statistical stability of the observations on the limited number of sources which the TPT was able to track. Unfortunately, a succession of severe rain and wind storms had an extremely adverse effect on the operation of the COCOA-Cross telescope and not only produced major interruptions in the observational program and reduced its reliability during synoptic observation programs, but also necessitated the diversion of financial and manpower resources away from scientific analysis toward field maintenance and instrumental improvements which were made in an effort to improve the reliability of the telescope. Consequently the TPT proved to be a valuable back-up to fill gaps in the COCOA-Cross observations.

Improvements to the COCOA-Cross have been made both in its field hardware (d.c. control wiring, switches, general strengthening) and in its pointing and data collection hardware, bringing it closer to our goal of producing an instrument capable of sustained, uninterrupted IPS observation (Section 4).

Synoptic IPS observations were undertaken on both telescopes during the summer of 1976 (17 May-25 August) and the fall of 1977 (18 November-13 December). These observations, in which measurements were made of the IPS spectrum, coupled with the earlier (1974) measurements of the IPS index (rms variation in intensity), have lead to the conclusion that, using the techniques already developed, prediction of geomagnetic activity is possible with a lead time of about 24 hours (Section 2).

Additional results include the association of spectral broadening with solar wind density enhancements near earth *(Gotwols et al., 1978;* and Appendix A), the detection of a solar wind velocity and turbulence latitudinal gradient out of the ecliptic plane *(Mitchell, 1978a,b;* and Appendix B), and the extension of our testing of the IPS prediction

technique to include a flare-driven plasma disturbance (from the great flare of November 22, 1977), and its associated geomagnetic activity (Section 3).

Finally theoretical considerations discussed in this report suggest a new technique which might extend the prediction lead time significantly, to 2 or 3 days (Section 5).

2. SCIENTIFIC RESULTS

It was determined, both from attempts to interpret scintillation index data in terms of prediction *(Erskine et al., 1978)* and from mathematical modeling *(Mitchell and Roelof, 1976)*, that in order to explore fully the feasibility of using IPS for prediction of geomagnetic disturbances, power spectral analysis of the intensity fluctuations was highly desirable. The need for spectra was based both upon the dependence of the frequency of the intensity fluctuations on distance to the scattering medium, which was essential information for prediction, and upon the increased ability to detect radio frequency interference (a serious source of contamination in the scintillation index data). The exploitation of this frequency dependence is discussed briefly in the Data Analysis Section, and more completely in *Gotwols et al., 1978.*

Therefore the construction of a high speed data acquisition system (DAS) was completed at APL, resulting in a system which functioned nearly flawlessly and which included the capability of simultaneously recording 10 sample per second data both on the COCOA-Cross and on the University of Maryland TPT radio telescopes. This system is described more fully in Appendix A. Also at APL an extensive software development effort was undertaken to reduce the raw data to power spectra suitable for analysis (example, Appendix A, Figure 8).

The first data set obtained was recorded using the APL DAS in June, July and August of 1976, reduced and analyzed at APL, and prediction feasibility possibilities were reported in the Interim report, Appendix A.

A previous attempt in using IPS for prediction concentrated on the analysis of a 1974 data set which included only synoptic scintillation index, with no spectra. This was found to be very noisy data, and the use of spectra in the 1976 data was a marked improvement over the technique of using scintillation index. In fact, an attempt was made to use index for prediction independent of the spectral data for the 1976 observations, with noteable lack of success. In analyzing the 1976 spectral data, we concluded at that time that given continuous synoptic observations on a large number of sources, particularly sources in the ecliptic plane,

prediction of geomagnetic disturbances could be achieved with moderate confidence about one day in advance. Since that time we have conducted another observation program during October 1977 using the only North-South arm of the COCOA-Cross on a reduced number (~ 20) radio sources. The analysis of this data, which was also recorded using the JHU/APL data acquisition system, is contained in this report, Section 3, and yields the same conclusion, however now documented for a large solar flare initiated disturbance (not encountered in the 1974 or 1976 data which were dominated by corotating structure). Again, a total fluctuation power parameter similar to scintillation index failed to produce as positive a result as the spectral analysis did.

The 1976 data set also yielded four scientific papers: *Cronyn et al., 1978; Gotwols et al., 1978* and *Mitchell, 1978a,b*. The contents of the *Gotwols et al., 1978* paper were similar to the analysis in Appendix A, in which broadening of the spectra was correlated with solar wind structure and geomagnetic activity, while scintillation index was found to be so noisy as to be of little or no use in prediction.

To give an idea of the other scientific results which came out of the 1976 data set, we describe the technique and results from *Mitchell 1978a* in Appendix B. The results from the 1977 observations will now be discussed in the following section.

3. SCIENTIFIC ANALYSIS OF 1977 OBSERVATIONS

During the upgrading of the COCOA-Cross radio telescope, there was a period between November 18 (day 322) and December 13 (day 347), 1977 over which it was possible to obtain nearly continuous synoptic observations on up to twenty-two radio sources which yielded usable IPS spectral data, using just the north-south arm of the array. This configuration resulted in a broad east-west beam pattern with typical source transits of $\sim$ 40 minutes. Although this configuration necessitated observations on a reduced number of sources, the increased time of observation of a given source allowed us to obtain spectra with excellent statistical stability. We have analyzed the data both in terms of (a) the IPS power spectrum and (b) the total integrated scintillation power.

a. Spectrum Analysis

The spectra were parametrized by ν_3, the frequency at which the power drops 3-dB below the low frequency plateau. Due to Fresnel diffraction effects and to source angular diameter dependence the high frequency portion of the spectrum is dominated by the near-earth interplanetary medium ($\leq$ 0.3 AU) while the low frequency portion of the spectrum is more sensitive to the more distant medium. The source angular size, θ, attenuates intensity fluctuations due to medium irregularities of angular sizes smaller than the source, i.e., fluctuation frequencies above $\nu = V_\perp / \pi\theta L$. The Fresnel frequency $\nu_f = V_\perp (\pi\lambda L)^{-\frac{1}{2}}$, the frequency below which the fluctuation spectrum is flat for a power-law electron density turbulence spectrum, also increases with decreasing distance along the line of sight, L. In these relations, λ is the radio frequency wavelength and $V_\perp$ is the solar wind velocity projection perpendicular to the line of sight. We attempt to exploit this distance dependence by using a measure of the width of the flat, low frequency portion of the spectrum (ν_3) as an indicator of the distance between earth and a solar wind disturbance which dominates the scintillation. This technique is discussed in detail in *Gotwols et al., 1978.*

In Figure 1 we compare the evolution of the width of ν_3 with Kp index. The radio sources used are listed from top to bottom in order of their observation times from the beginning to the end of the UT day, and the magnitude of ν_3 is plotted logarithmically. When two values of ν_3 are plotted on a given day, the spectrum was what we term "two-component", i.e., it falls off from the low frequency plateau approximately as a power law, then flattens due to an enhancement at higher fluctuation frequencies before falling off again to the white noise background level.

Ideally we would have an ecliptic point source to the east and sunward of the earth with 24 hour/day monitoring of the scintillations to watch the change in the spectrum caused by the evolution in the density fluctuation profile associated with approaching solar wind disturbances. Instead we have finite diameter sources each of which we can watch only for about 40 minutes/day and none of which lie in the optimum position (at this time of year) for early detection of a corotating solar wind disturbance. In fact the better scintillators (3C48, 3C123, 3C144, 3C196, 3C216) lie in the anti-sunward direction and to the west. Therefore in exploring feasibility of prediction we will generally examine the width of the spectra of these western sources after the onset of solar wind-triggered geomagnetic activity to look for the signature of the solar-wind disturbance as it corotates away from the earth. Since at 34 MHz we primarily respond to the density increase preceding the rise in velocity in a solar wind stream-stream interaction region *(Erskine et al., 1978)*, the region is not extended and we expect similar signatures in the west for a receding disturbance to that in the east for an approaching disturbance.

The first event we will examine is probably not corotating. A flare on day 326:09 (November 22) is most likely responsible for the geomagnetic disturbance which began with an SSC on day 329. In Figure 2, we have displayed the sources observed in ecliptic coordinates to show the detection of this disturbance. Open circles are narrow spectra, closed circles are broad spectra, and half-filled circles are for spectra with moderate high frequency enhancement. A data gap for all sources but 3C144 on day 329 complicates the analysis, but we would expect to see the event first in the sunward hemisphere. Of the sources in that direction, only

three (3C273, 3C298 and 3C324) were monitored just prior to the SSC. Of these, 3C273 does not show a strong signature, but it does have a marginally significant high frequency component on day 328 (not recorded in Figure 1), consistent with the approach of the disturbance. 3C298 shows an increase in ν_3 from day 327 to 328 and 3C324 shows a relatively high ν_3 on day 328, both consistent with ~ 1 day prediction of the event. It can be seen in Figure 2a that all three of these sources lie at elongation angles small enough that strong scattering may have an important effect on the spectrum. In either weak or strong scattering we would expect broadening, however. On day 329 we have data on only one source, 3C144. The observation took place before the SSC, and as 3C144 is in the anti-solar direction, the narrow spectrum observed is consistent with the disturbance not yet having reached the earth. Figure 2a shows the observations for 24 hours before the SSC.

After the SSC, the Kp index, plotted in Figure 1, rises and remains elevated for half a day and somewhat enhanced until early on day 331 over which period virtually all the sources observed display scintillation with broad spectra (see also Figure 2b), indicating that the earth is immersed in solar wind turbulence. Although the Kp index decays early on day 331 and the interplanetary disturbance has probably propagated beyond the earth, the spectra for the anti-solar sources 3C13, 3C48, 3C68.2, 3C144, 3C161 and 3C196 remain broad on day 331 (Figure 2c) as the disturbance no longer engulfs the earth but is still near the earth ($\leq$ 0.3 AU). This argues for this technique's ability to detect a disturbance up to 0.3 AU from earth. On day 332 the spectrum for 3C48 (a small diameter source and therefore sensitive to turbulence at larger distances than most of the other sources) still exhibits a high frequency enhancement, but all the other sources return to narrow spectra.

Figure 2 shows the evolution of the response to this disturbance and indicates how we can detect turbulence in the solar wind before it arrives at earth (Figure 2a), when it surrounds the earth (Figure 2b), and after it has gone past the earth (Figure 2c).

There is a small enhancement in Kp on day 334, which was preceded by several hours by a broad spectrum on 3C409 looking to the east (Figure 1). Actually, this is the second consecutive day that the spectrum for 3C409 increased in width, though it is hard to say whether all of the broadening

can be attributed to the disturbance which apparently corotated past the earth on day 334, since this event is closely followed by a much larger enhancement of Kp and SSC late on day 335 and continuing to the end of day 336. Of the eastward-looking sources, on which we would expect to see broadened spectra as a corotating disturbance approaches from the east, only 3C459 sees the disturbance early on day 335, before it reaches earth. We do not have data on the other eastern sources (4C+21.53, 3C409, 3C380), and we cannot go more than one day back to look for the signature of this disturbance due to the dominance at that time of the day 334 disturbance.

On day 336 nearly all the sources display broad spectra, reflecting the proximity of the turbulence which engulfs the earth at this time. The next day the spectra return to normal width with the exception of 3C216 and 3C254 which still appear to be responding to the solar wind disturbance which has corotated to the west, again demonstrating our ability to detect the disturbance even when it has corotated away from the earth.

After this event the data is not very continuous. There is an enhancement in Kp index on day 339 which is well associated with a broadening in the spectrum of 3C298, and another enhancement in Kp on days 345, 346, and a little on 347, which causes the spectra of several sources to broaden. Of these latter 3C216 shows a broader spectrum on day 347 (after the Kp index has diminished somewhat) than it does on day 345 at the height of the event, making it a good candidate for prediction during the time of year it lies to the east.

In an attempt to characterize the broadening of a spectrum due to enhancement at the high frequency end in a more general way, we devised in Figure 3 a qualitative display of the relative change in the width of the spectrum for a given source from one observation to the next. In this figure, we show an increase (decrease) in spectral width from observation 1 to observation 2 by an arrow directed from (to) the day of observation 1 to (from) the day of observation 2. A double-ended arrow means no change, and a heavy arrow means a large change. Observations on a given day run horizontally; on a given source, vertically, and the sources are listed from left to right in order of their observation on a given day. Periods of disturbed geomagnetic field ($Kp > 3$) are marked at the beginning by a D, and followed by a Q (for quiet, $Kp \leq 3$) at the time when the disturbance dies away.

This characterization removes the confusion generated by one- and two-component spectra, and since it is the change in spectral width from one observation to the next which is recorded in this approach to prediction, rather than the absolute width of the spectrum, long term trends such as elongation angle dependence are minimized.

A glance at Figure 3 will tell which days are of interest. Any day which shows a large number of arrow-heads pointed toward it would be expected to be an "all-sky" day (a term coined by *Erskine et al., 1978*, to describe a day when the earth is immersed in turbulence and most sources which can scintillate do scintillate, in all directions). Thus on this plot days 330 and 331, 334, 336, 345 and 347 stand out as "all sky" days, when we would expect geomagnetic activity. For prediction, we must examine the figure more closely, being careful to separate eastern and western sources and looking for increasing width of spectra in the east and decreasing width in the west for corotating disturbances, or observing separately the change in width of sunward and anti-sunward sources for radially propagating disturbances.

On day 328 the sunward source 3C273 shows a decrease in width from the day before, in spite of the small high frequency component referred to previously. This decrease in width, which is mainly in the low frequency portion of the spectrum, may be due to the presence of more turbulence to the west on day 327, not seen at earth. There was only one observation made on day 329, and that was in the anti-sunward direction where 3C144 gave a narrow spectrum. A few hours later there was an SSC, and broad spectra were recorded on most sources observed during days 330 and 331. In addition, many of the sources in the anti-sunward direction (3C48, 3C196, 3C216, 3C238) show decreasing spectral widths over the next two days, consistent with the increasing distance from earth to the disturbance.

There is an all sky increase on day 334 due to the small disturbance that day, but any trend towards decreasing width of the spectra of western sources is obscurred after one day by the arrival of a large disturbance causing an SSC late on day 335. This disturbance results in an all sky day on day 336, and several western sources for which we have data (3C48, 3C216, 3C238, 3C254, 3C263.1) show decreasing spectral widths

up to day 338. Of the other western sources for which we do not have data continuously during this period, only 3C123 is not consistent with this interpretation.

Again early on day 345 the Kp index is elevated, and the arrows indicate an all-sky enhancement. As we can see, after the missing data on day 346 we continue to show spectral broadening on day 347. This may be detection of the disturbance which triggered the day 345 event or it may be a separate disturbance. The Kp index remains somewhat elevated throughout the period, though it is lower on day 347 than on day 345.

b. Scintillation Power

Now we will examine Figure 4, which is a plot of I/I_{max}, where I_{max} is the maximum I observed for a given source over the course of the observation period, and I is a measure of the normalized spectral fluctuation power:

$$I = \sqrt{\frac{VRMS^2 - 3.15\ V23\ Hz^2}{V23\ Hz}}$$

$VRMS^2$ is the integrated power over the full spectrum and $V23\ Hz^2$ is the power integrated between 2 Hz and the anti-aliasing filter at 3 Hz, a portion of the spectrum containing virtually 100% white noise. The 3.15 multiplier is an empirical constant chosen such that I = 0 for white noise. This quantity has the disadvantage of being sensitive to the telescope response, so that the calculated I's should be normalized by the height of the source transit on that day. This was not done for this data set due to the large measurement uncertainty in measuring the transit heights for many of the weaker sources. We did compare the daily response on the strong source 3C144 and normalize the 3C144 points to it. We found a general decrease in sensitivity of the instrument over the period by about a factor of 3, but it was gradual and did not seriously distort short term (3-4 day) trends in the data.

If we look at 3C196, 3C216, 3C238 and 3C254, they all show a decreasing trend from day 330 to day 332 or 333, which may be linked to the scattering region moving farther from earth and producing less total fluctuation in intensity due to the increasing influence of source size in quenching the scintillations. Other sources with I-dependence consistent with this trend are 3C459, 3C48, 3C68.2 and 3C123. The exceptions are 3C144 and 3C161, but a close examination of the 3C144 spectrum on day 332, the most drastic deviation from the trend, revealed a strong possibility of contamination by radio frequency interference. The slight increase between days 330 and 331 on 3C161 and 3C144 is probably due to spatial structure of the disturbance, i.e., the turbulence may have increased between 3C161 and 3C196 on day 330. Note that unlike the spectral width data, there is no apparent indication of the approach of this event in the I-dependence of 3C298 and 3C324 later on day 328. This lack of signature may be due to strong-scattering, which is a much more difficult phenomenon to recognize and interpret in the total fluctuation power than it is in the spectral data.

On day 334 there was an increase in (normalized) I on most of the sources which we observed that day, consistent with the rise in Kp index on that day, and then a decrease on day 335 leading into a large increase on nearly all sources on day 336. The one exception to this pattern for which we had data continuously from day 333 to 337 was 3C459. This source displayed increases on each day from day 334 to day 336, which we interpret as first the day 334 increase seen by the other sources, but then instead of returning to a relatively low level as in the case of the western sources, its fluctuation power is enhanced further on day 335 by the influence of the approaching corotating turbulence which causes the day 336 enhancement for the other sources. Both the day 334 and 336 enhancements are "all-sky" days (as in *Erskine et al., 1978*), and the pattern following the day 336 enhancement does not show a monotonic decrease as clearly as the ν_3 plot does.

The remainder of the data is too sparse to analyze to any degree of precision. One event should be mentioned, though. Most of the sources were enhanced on days 345 and 347 (there was no data on day 346), consistent with the increase in Kp on day 345 and the continued influence on the western sources of the associated solar wind disturbance two days later on day 347.

We conclude that in looking at the data set in terms of both spectral shape (ν_3) and scintillation power (I) as measured by the COCOA-Cross in 1977, interplanetary scintillations at 34 MHz were useful for prediction of geomagnetic activity at best about one day in advance, provided the radio source locations are optimum for prediction, i.e., sunward and to the east, but not in strong scattering. It maybe that instrumental and analytical techniques not employed here, such as that discussed in Section 5, will improve the lead time of the prediction using 34 MHz radio scintillations.

4. COCOA-CROSS INSTRUMENTAL UPGRADING

a. Field Hardware

For orientation purposes, simplified schematics of the north (or south) and east (or west) telescope arms are shown in Figures 5 and 6. It should be understood that the COCOA-Cross was originally constructed with a grant of $30,000 in 1972 from NASA, and numerous economies in materials and construction techniques had to be employed which resulted in poor reliability and vulnerability to long term deterioration. For example, all the d.c. lines which controlled the telescope phasing diode switches were grouped in surplus multiconductor cables which lay directly on the ground. After four years of exposure to strong sunlight, high temperatures, rain and submersion in alkali mud, the cable insulation was cracked. Consequently extensive, difficult-to-locate shorts developed after each rain. The diode switches, consisting of a diode, 3 capacitors and 2 resistors, were constructed on small acrylic plastic blocks and dipped in epoxy. Again, after four years of severe environmental exposure the epoxy coating had been largely sand-blasted away, causing the diodes to crack and component connections to corrode and fail.

Thus, on the basis of the condition of the d.c. control lines ans switches, and the over-riding requirements for a high reliability instrument to take 24 hour/day, 365 day/year IPS observations, we decided to install new d.c. control lines and design and install new phasing control diode switches. The new d.c. control lines are open wire lines, entirely elevated above the ground (see Figure 7). These lines are not only above any reasonably predicted water level but also, because the lines are open, shorts and breaks can be readily located and fixed without having to cut into heavy jacketed multiconductor cable (as was necessary for the old d.c. control lines). Even if the lines should be submersed in an extraordinary flood, they can dry out quickly, unlike the multi-conductor cables which tended to trap water inside the outer jacket. A total of approximately 30 miles of new, elevated, open wire d.c. control line was installed by August 1977.

All of the diode phasing switches were also replaced by a total of approximately 1600 opaque, fully encapsulated switches (Figure 8).

In addition to the switches and control lines, we also installed preamplifiers at the output of each bank of 8 antenna elements to improve the overall signal-to-noise ratio of the telescope (Figure 9). Measurements taken on just the north-south area in November-December 1977 showed that the signal-to-noise ratio in the IPS power spectrum was 3 db higher than for the entire telescope before the new bank and buffer amplifiers were added. The signal-to-noise ratio for the entire telescope is 6 db higher than for the north-south area alone so we anticipate that the total improvement in signal-to-noise ratio will be about 9 db. A total of 16 preamplifiers were installed in the north-south arm, and 32 in the east-west arm. Circuitry to enable on-off control of each individual preamplifier was also installed.

b. Control Hardware

In the original d.c. control line system each type of switch (for example, all north-south arm line/fan position 2 switches) was connected to its own indivudual d.c. control line which was either turned on to forward bias the switches, or turned off which, for the silicon diode switches, was effectively back-biasing the switch. That is, the control voltage was unipolar.

However, to reduce the number of new d.c. control lines by a factor of 2 and thereby reduce installation and maintenance time and expense, we decided to employ a bipolar switch control voltage on each line for which one polarity would serve to forward-bias one member (i.e. N-S line/fan 2) of a pair of switches and back-bias the complementary member (i.e. N-S line/fan 1); reversing the polarity reversed the switch pair combination (i.e. to N-S line/fan 2 off, N-S line/fan 1 on). The old beam-steering control system was designed to provide only unipolar switching voltages. In an effort to provide a simple unipolar-to-bipolar switching voltage conversion we attempted to use a simple reed-relay interface. The solenoids were controlled by the original unipolar switching voltage while the armature switched between + and - 48 volts. Unfortunately the reed relays had a poor reliability record (due in part to the highly capacitive d.c. control line main feed cable), and very occasional short circuits (i.e. once during the night in a wind storm) would blow the protective fuses, rendering the beam steering system useless. Although the observations of November-December 1977 were taken using the reed relay interface it necessitated an inordinate amount of attention and d.c. control line current monitoring to insure proper operation.

We therefore felt that it was essential to undertake the design of new electronic solid-state switches which would:

1. Provide protection against external shorts via current limiting, not fusing, so that occasional shorts would have no permanent (i.e., fuse-blowing) effect on the beam steering system;

2. Provide immediate visual and electrical flags to indicate deviations in total switch current draw (both excesses, or shorts, and deficiencies, or breaks);

3. Be easily interfaceable to the Poly 8080-based processor.

The new switch drivers not only have features (1.) - (3.) but also have a controllable disable to turn off 1 or more selected d.c. control lines for test purposes, and a built-in dual beam capability to provide for essentially instantaneous switching between 2 different beams without having to transfer complete beam pointing information each time. One of the switch driver cards is shown in Figure 10.

The switch driver cards are controlled by the Poly 8080-based microprocessor system through a single master interface card (Figure 11) and a switch driver control card (1 for each 6 switch drivers; see Figure 12).

c. Poly 8080-Based Microprocessor

Repeated mechanical failures of the card reader and paper tape punch and their associated continuing maintenance costs and the major interruptions to the observing program caused by d.c. control line faults and the necessity of carrying out long, tedious diagnostic procedures on the control lines compelled us to consider the use of a completely non-mechanical telescope control and data acquisition system based upon the new inexpensive microprocessor chips. The system requirements were four-fold:

(1) Replace the card reader and directly control the upgraded main beam switching network;

(2) Sense malfunctions in the telescope itself;

(3) Replace the punch unit and record the data on a more reliable audio cassette recorder;

(4) Upline, or transfer, to the NOVA computer system the data stored on the audio cassette.

The final hardware configuration of the new system consists of a Poly 8080-based micro computer with 16 K bytes of RAM, a cassette modem, a video monitor, a cassette recorder, a keyboard, and a parallel-serial I/O handler. The micro system is connected via a 4800 band serial line to the NOVA computer system. An 8-level vectored priority interrupt and a real-time clock are part of the hardware architecture.

An overall block diagram of the beam-pointing and data acquisition system is shown in Figure 13.

The software system was developed in assembly language to optimize memory use and to take full advantage of the interrupt hardware. The customized real-time operating system used a software sidereal clock to control the various functions of the telescope, to gather data and record it, and to respond to external commands to perform other tasks - such as receive a new observing program, replay the data accumulated on the audio tape, reset the clocks, modify the beam positioning, page through the observing list, etc. The microcomputer is not a slave to the NOVA; rather, the two systems communicate as peers. This allows the telescope to function independently of the data processing and scientific calculations being carried out off-line

by the NOVA. The micro is a system dedicated to telescope monitoring and control, and data acquisition, while the NOVA serves as a general purpose computational facility.

The observing procedure is as follows: Sources are selected from the Cambridge IPS catalog or other lists of sources which are known to be of small angular size and display IPS at 34.3 MHz. The coordinates are entered into a NOVA program called ALLIN1 which produces processed direct coordinates, elliptic and galactic coordinates, and the beam steering switch settings. These data are recorded on a magnetic tape for transfer at a convenient time to the memory of the microcomputer control system. The telescope observes the sources on the observing schedule, which may include up to 200 sources. The radio intensity and phase information channels are digitized and the data temporarily stored in the computer memory. At the present data rate of one channel/5 sec., the memory buffer is dumped onto audio cassette tapes approximately once an hour. A standard 30 minute cassette tape provides a data storage capacity of at least 5 full days. At a convenient time this audio cassette data tape is rewound and read back into the microcomputer which uplines the data via the serial connector to the NOVA computer. This process does not interrupt the normal observing of the telescope. The data is recorded in NOVA compatible format for off-line analysis. During the observing procedure at regular intervals the different control lines are checked for undercurrent, caused by defective array switches or broken lines, and overcurrent, often caused by short circuits. This error information is presented on a CRT monitor to inform the observer of possible maintenance problems.

The on-site data reduction procedures available to the observer have been improved significantly. Not only has the inconvenience of paper tape handling been eliminated, but a video terminal installed. Data can be quickly examined, manipulated, and the final results displayed on a Versatec printer/plotter. New programs have been prepared to aid in the Fourier analyis of the data and in theoretical calculations pertinent to the solar wind and IPS. This capability formerly was not present at the site itself.

5. EVALUATION AND FUTURE PLANS

We emphasize that we have by no means exploited the full performance and operational capability of the telescope, and that with a longer data base of higher signal-to-noise radio observations on more sources, which the telescope is now capable of, the lead time may be extended. That is, we feel that the feasibility of making predictions based on IPS activity has not been fully explored during this contract period, but the physical reliability of the telescope has been drastically improved, array malfunction monitoring instrumentation has been installed, and data acquisition and processing is sufficiently highly automated that the small staff of scientific personnel stationed at Clark Lake on the COCOA-Cross project can realistically expect to keep up with the large number of daily observations and parameters (4 data parameters/sources; ~ 125 sources/day going to ~ 200/day).

All of the new d.c. control lines, amplifiers, diode phasing switches and switch drivers, the Poly 8080-based microprocessor system and the control, data acquisition and data processing software were developed and installed only because they were absolutely essential to the project mission of studying the feasibility of using IPS to forecast geomagnetic disturbances. The size of the telescope, harshness of environment, volume of observational data and lack of skilled manpower made necessary the hardware and software additions and improvements. It was unfortunate that the initiation of the feasibility study coincided with the wettest and most destructive weather of the past 16 years (see Appendix C).

We have previously *(Roelof et al., 1977-AFGL Final Report)* discussed the fact that for a source of angular size θ, at a given frequency ν in the power spectrum, contributions to fluctuation power will be strongly attenuated at distances $\geq L$:

$$L = V_{\perp}/\pi\theta\nu = 0.18\ \text{AU}(V_{\perp}/400\ \text{km s}^{-1})/(\theta''\nu)$$

so that for typical $V_{\perp}/400 \approx 1$, $\theta'' \approx 1$ and $\nu = 0.5$ Hz, $L_{max} \approx 0.35$ AU. The measurements made to date, i.e., scintillation index for the chart record data and frequency scale for the power spectra, are strongly

influenced by near-by turbulent structure. However, if absolute power spectral density normalized by (source response)^2 is measured at low frequencies, i.e., $\sim$ 0.15-0.2 Hz, then the maximum distance of response is extended to $\sim$ 0.7 AU for $\theta \sim 1.0''$ which means that the lead time for corotating density enhancement warnings is extended to $\sim$ 3 days. As we resume operation with the up-graded COOOA-Cross facility we shall be monitoring total fluctuation power at $\sim$ 0.2 Hz to exploit this possibility of extending lead time.

6. SUMMARY

The program undertaken to study the feasibility of prediction using IPS was conducted as a collaboration between the University of Iowa group at the COCOA-Cross Radio Telescope installation at Clark Lake Radio Observatory which provided manpower for up-grading the COCOA-Cross array and the use of the instrument observations, and The Johns Hopkins University/Applied Physics Laboratory group. The latter assumed responsibility for data collection and analysis, including mathematical modelling, construction of a data acquisition system, observers on site, data reduction and analysis, and publication of scientific results both individually and jointly with members of the Iowa group.

Damage to the COCOA Cross as a result of abnormal rainfall, and the continued vulnerability of the telescope to rain damage accompanied by extended periods of down time, made it necessary to replace the original diode phasing switches and multiconductor d.c. control lines with opaque, fully encapsulated switches and elevated open wire, d.c. control lines. These changes, combined with the limitations and failures of the card-reader controlled main beam steering system and the punched paper tape data acquisition system, compelled us to develop and produce new, bipolar, solid-state switch drivers controlled by a microprocessor which also serves to acquire the low rate data previously taken on the punched tape system.

Bank and buffer amplifiers which have significantly improved the signal-to-noise ratio of the telescope have been installed.

The improvements in field hardware and control, monitoring and data acquisition hardware and software now make it possible to undertake a far more intensive prediction feasibility study than was possible at the beginning of the contract period. The telescope is now also far less vulnerable to rain and wind damage, and far easier to maintain.

As a result of the damage to the telescope caused by severe weather conditions, the extensive data set anticipated at the inception of this program was never realized. Two separate sets of observations

were obtained, in the summer of 1976 and the fall of 1977. As continuous synoptic observation is essential to the application of IPS to prediction, the usefullness of the observations obtained was further limited by data gaps caused by telescope malfunctions and radio frequency interference (both of which should be greatly reduced after the recent improvements). The feasibility of using IPS for prediction is therefore based upon rather undefinitive data, and it is our recommendation that further observations be carried out to confirm the results of this study, namely that prediction using this technique is feasible under favorable conditions with lead times up to and sometimes exceeding 24 hours. During the second observation period we extended the application of the technique beyond purely co-rotating solar wind disturbances to include flare associated disturbances which resulted in geomagnetic activity.

The use of the spectra of the intensity fluctuations has been fundamental to the understanding of this technique. Furthermore, application of the spectral broadening technique, developed in the course of this study, has led to significant scientific results including: the association of the major component of the IPS index response and spectral broadening at 34 MHz with density enhancements in the solar wind; and the detection of a positive heliolatitude gradient in solar wind velocity associated with a possible negative gradient in solar wind turbulence.

Though it is desireable to continue the acquisition and reduction of some data for spectral analysis, the work (both analytical and theoretical) conducted during this study has provided us with the understanding and insight into the frequency dependence of the intensity fluctuations necessary to make informed decisions on measuring more easily obtained parameters which will be useful for prediction. Therefore on the basis of observations to date, and supporting theoretical analysis, we have decided to record not only the total source response, fluctuation power from 0.1 to 1.5 Hz and first spectral moment (which like ν_3 is a measure of spectral width), but also source-response-normalized fluctuation power at relatively low fluctuation frequencies, i.e., $\sim$ 0.1-0.3 Hz. We anticipate that such measurements will yield predictive measurements with IPS activity leading geomagnetic activity by upwards of two days.

PERSONEL

The Johns Hopkins University/Applied Physics Laboratory

Bruce L. Gotwols, Senior Physicist
Donald G. Mitchell, Post-Doctoral Research Associate[1]
Edmond C. Roelof, Senior Physicist

The University of Iowa

Willard M. Cronyn, Associate Research Scientist
James J. Rickard, Research Associate
Stanley D. Shawhan, Associate Professor

[1] Research Associate, University of Iowa, 1 February 1977 - 1 April 1978

We would also like to acknowledge the gracious cooperation of Professor W. C. Erickson, who arranged the use of the University of Maryland TPT array at CLRO by Gotwols and Mitchell during the COCOA-Cross observations in 1976 and 1977.

PUBLICATIONS AND PRESENTATIONS

In addition to the publications marked by an (*) in the list of references, the following papers on this research were presented at the Fall 1976 and Spring 1977 National Meetings of the American Geophysical Union:

Erskine, F. T., W. M. Cronyn, S. D. Shawhan, E. C. Roelof and B. L. Gotwols, Interplanetary scintillation at large elongation angles: Response to solar wind density structure, *EOS*, *57*, 998, 1976.

Gotwols, B. L., D. G. Mitchell, E. C. Roelof and W. M. Cronyn, Power spectra of interplanetary radio scintillations observed at 34.3 MHz, *EOS*, *57*, 999, 1976.

Gotwols, B. L., E. C. Roelof, W. M. Cronyn, D. G. Mitchell and W. C. Erickson, Synoptic spectral analysis of interplanetary radio scintillations May-August 1976, *EOS*, *58*, 485, 1977.

REFERENCES

Publications resulting from research under this contract are indicated by an asterisk (*).

(*) Cronyn, W. M., S. D. Shawhan, J. J. Rickard, D. G. Mitchell, E. C. Roelof and B. L. Gotwols, IPS activity observed as a precusor of solar induced terrestrial activity, Proc. NATO/AGARD Symposium *Operational Modeling of the Aerospace Propagation Environment* (Ottawa), in press, 1978.

(*) Erskine, F. T., W. M. Cronyn, S. D. Shawhan, E. C. Roelof and B. L. Gotwols, Interplanetary scintillation at large elongation angles: Response to solar wind density structure, *J. Geophys. Res.*, *83*, in press, 1978.

(*) Gotwols, B. L., D. G. Mitchell, E. C. Roelof, W. M. Cronyn, S. D. Shawhan and W. C. Erickson, Synoptic analysis of interplanetary radio scintillation spectra observed at 34 MHz, *J. Geophys. Res.*, *83*, in press, 1978.

Mitchell, D. G. and E. C. Roelof, A mathematical analysis of interplanetary scintillation in the weak scattering approximation, *J. Geophys. Res.*, *81*, 5071, 1976.

(*) Mitchell, D. G., Interplanetary radio scintillation at 34 MHz: Evidence for a solar wind latitude gradient, submitted *J. Geophys. Res.*, 1978a.

(*) Mitchell, D. G., Analysis of interplanetary scintillation spectras at large elongation angles, submitted *Planetary and Space Science*, 1978b.

Roelof, E. C., B. L. Gotwols, D. G. Mitchell, W. M. Cronyn and S. D. Shawhan, Use of interplanetary radio scintillation power spectra in predicting geomagnetic disturbances, Final Report to the Air Force Geophysical Laboratory, *AFGL-TR-77-0244*, 1977.

FIGURE CAPTIONS

FIGURE 1 Plot of spectrum 3 dB frequency on a logarithmic scale versus day of the year for twenty radio sources. Kp index is plotted at the bottom for the same period, versus day of the month. Sudden storm commencements (SSC's) are indicated by a triangle both on the Kp plot and on the log (ν_3) plot between the sources whose observations bracket the SSC. Dashed lines connect points separated by more than one day. Points in parentheses are the second component of possible two-component spectra.

FIGURE 2 Ecliptic longitude plots for the day prior to and two days after an SSC on day 329:1200. Filled circles indicate large increases in ν_3 or broad spectra (for that source), half-filled indicate moderate increases in ν_3 or intermediate width spectra, and open circles indicate decreases in ν_3 or narrow spectra. On the day prior to the SSC (a) only sunward sources show broadening in response to the disturbance inside 1 AU. Following a data gap, day 330 and early day 331 (b) shows an all-sky day, with broad spectra in all directions as the earth is immersed in turbulence, and the following day (c) the broad spectra are almost entirely early in the day and in the anti-sunward direction, responding to the disturbance as it propagates beyond the earth into deep space.

FIGURE 3 Plot of the (qualitative) change in width of the spectrum from one observation to the next for 19 radio sources over the November-December 1977 observation period. Light arrows indicate a moderate change in spectral width, pointing toward the day with the broader spectrum. Heavy arrows indicate a large change in spectral width, and double-ended arrows indicate little or no change. D and Q designate the beginning of periods of disturbed and quiet geomagnetic field, respectively. Sudden storm commencements are indicated by a filled triangle placed on the day of occurrence, between the source observations which fall just prior to and just after the SSC.

FIGURE 4 Linear plot of normalized fluctuation power (I/I_{max}) versus time, with Kp index plotted below. Dashed lines connect points separated by more than one day. Sudden storm commencements are indicated by filled triangles placed on the day of occurrence between the source observations immediately preceeding and following (in time) the SSC. This is a measure similar to scintillation index, but is not normalized by the source intensity.

FIGURE 5 Simplified schematic of East (or West) arm branch feed system. All transmission lines are balanced open wire line. Lines are identified by number: within the column north-south lines 1-3; between columns, east-west lines 1-5. Antenna elements (V) are approximately 33 m long and oriented east-west. North-south separation, 6.55 m. Phase switching system same as in north-south arm. Two control lines are required for each of the 3 north-south lines, 3 are currently required to accomplish east-west pointing, and 2 (not shown) are required to accomplish north-south/east-west arm phasing for a total of 11 control lines. The original unipolar switches were replaced by 998 fully encapsulated switches controlled by bipolar switching voltages. Bank and buffer amplifiers were also installed. The switch and amplifier tasks were made possible by AFOSR support.

FIGURE 6 Simplified schematic of North (or South) arm branch feed system. All transmission lines are balanced open wire line. Lines are identified by number (1-8) on left. Antenna elements (V) are approximately 63 m long and oriented east-west. North-south element separation is 6.55 m. Appropriate phase for reversing switch (0° or 180°) is determined by polarity of line reversing switch control voltage, V_c, and similarly for the phase of the fan switch (0° or 90°). Each type of switch (for example all 32 north and south arm line 2, fan switch 2 diode switches) is controlled by its own individual d.c. control line. Since fan and reversing switch control voltages are required for each of lines 1-6, 3 real-time delay tap voltages are required on line 7 and 5 on line 8, and 3 control lines are required to set the phasing switches (not shown) between the north and south arms,

a total of 23 d.c. control lines plus a common return line are required for north-south arm beam pointing. The original unipolar switches were replaced by 608 fully encapsulated switches controlled by bipolar switching voltages. Bank and buffer amplifiers were also installed. Both switch and amplifier tasks were made possible by AFOSR support.

FIGURE 7 New d.c. control lines reflecting sun light. The lines are elevated at least 18 inches off the ground.

FIGURE 8 New, fully encapsulated phasing switches. Switch cable is connected to new d.c. control line.

FIGURE 9 Bank amplifier at output of East arm bank.

FIGURE 10 Switch driver board, 4 drivers/board.

FIGURE 11 Master interface board to connect Poly 88 microprocessor to control boards.

FIGURE 12 Control board for switch drivers. Each board contains 6 switches ($1\frac{1}{2}$ switch drive boards). It is connected through a bidirectional data line to a master interface. Each of the 13 control boards has a unique address set on the binary slide switches.

FIGURE 13 Block diagram of beam-pointing and data acquisition system. Source ID and coordinates are entered into the NOVA which then completes current celestial, ecliptic and galactic coordinates; phase up and transit times; switch settings; and miscellaneous control settings are computed by a NOVA program called ALLIN1. A printer listing and cassette tape containing data downlined to the Poly 88 are generated by the NOVA. Switch settings are distributed by the Poly 88 through an interface board to control boards and the switch driver boards. If phasing switch current draw is either lighter or heavier than present thresholds a flag is set which is passed to the Poly 88. The flags, time and 4 channels of data are recorded on a digital cassette tape for convenient uplining to the NOVA for final processing and plotting.

THE JOHNS HOPKINS UNIVERSITY
APPLIED PHYSICS LABORATORY
LAUREL, MARYLAND

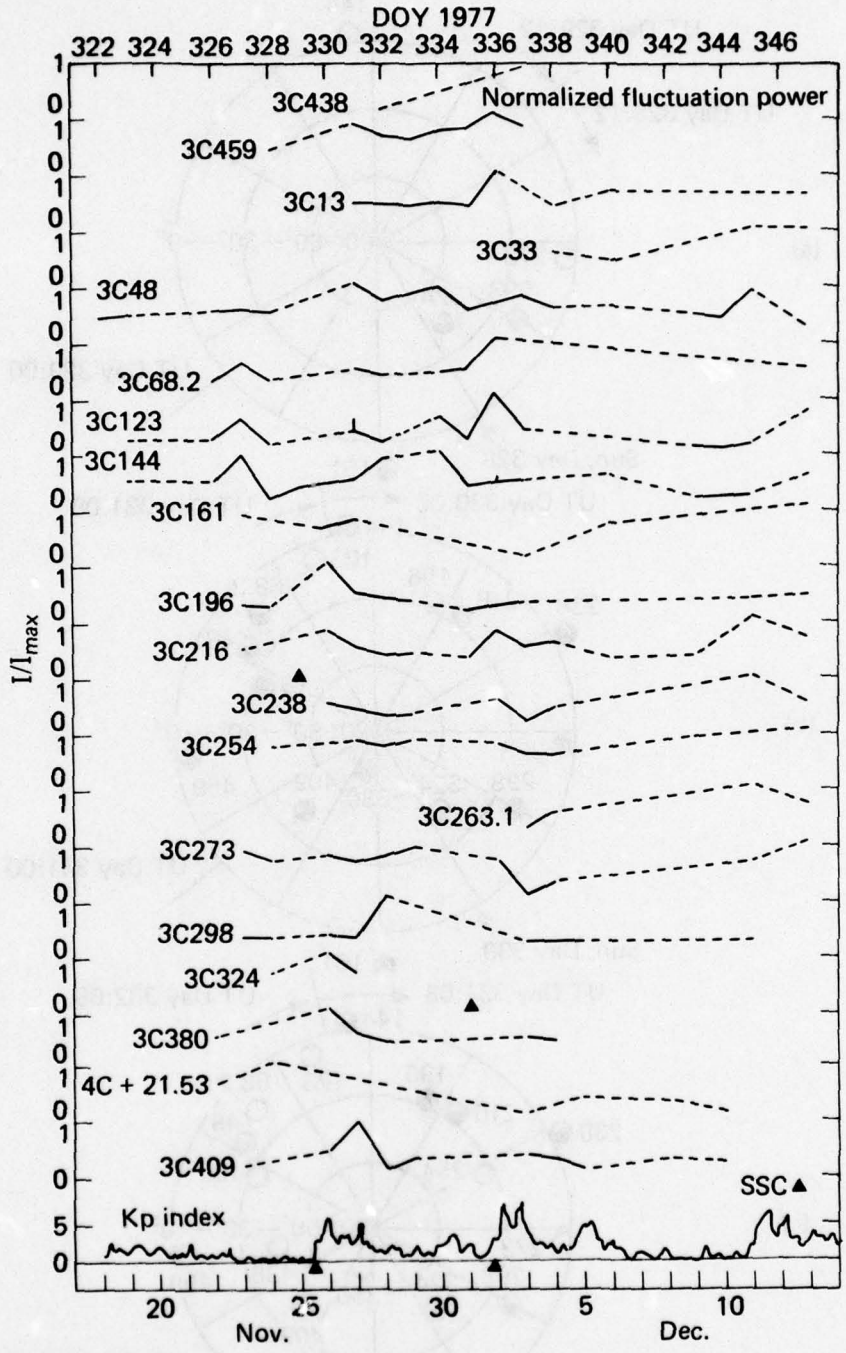

FIGURE 1

THE JOHNS HOPKINS UNIVERSITY
APPLIED PHYSICS LABORATORY
LAUREL, MARYLAND

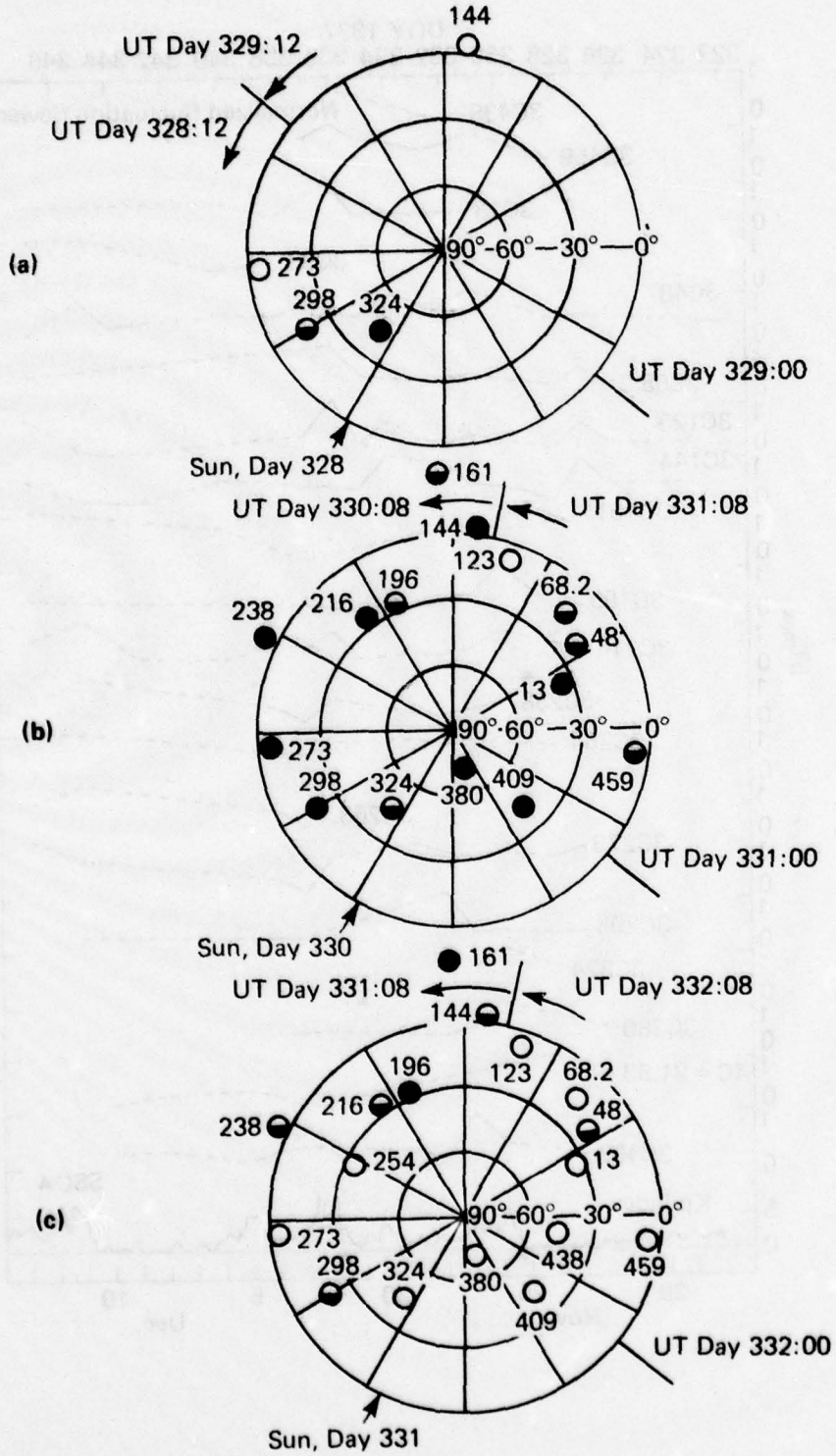

FIGURE 2

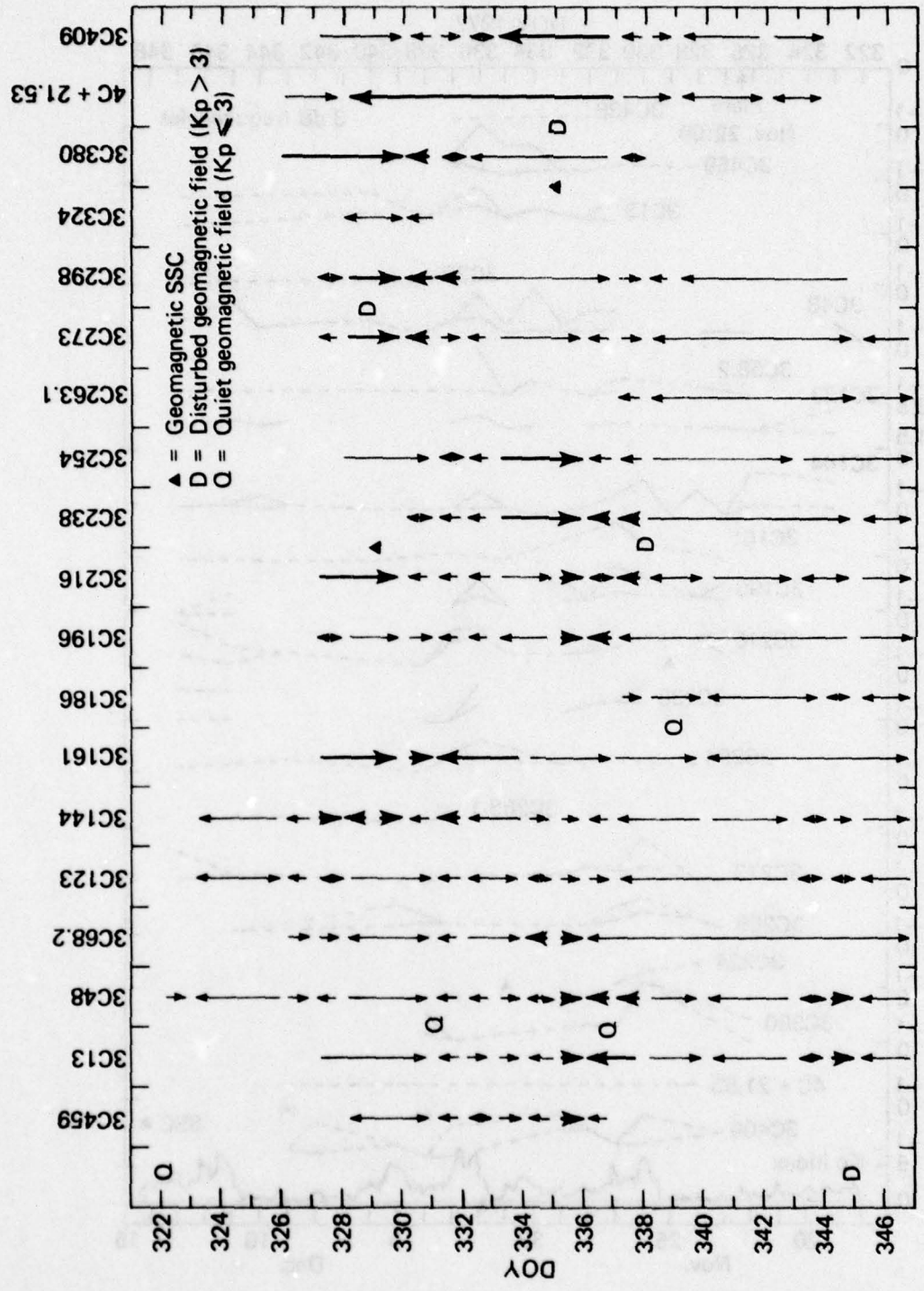

Qualitative change in breadth of sequential power spectra

FIGURE 3

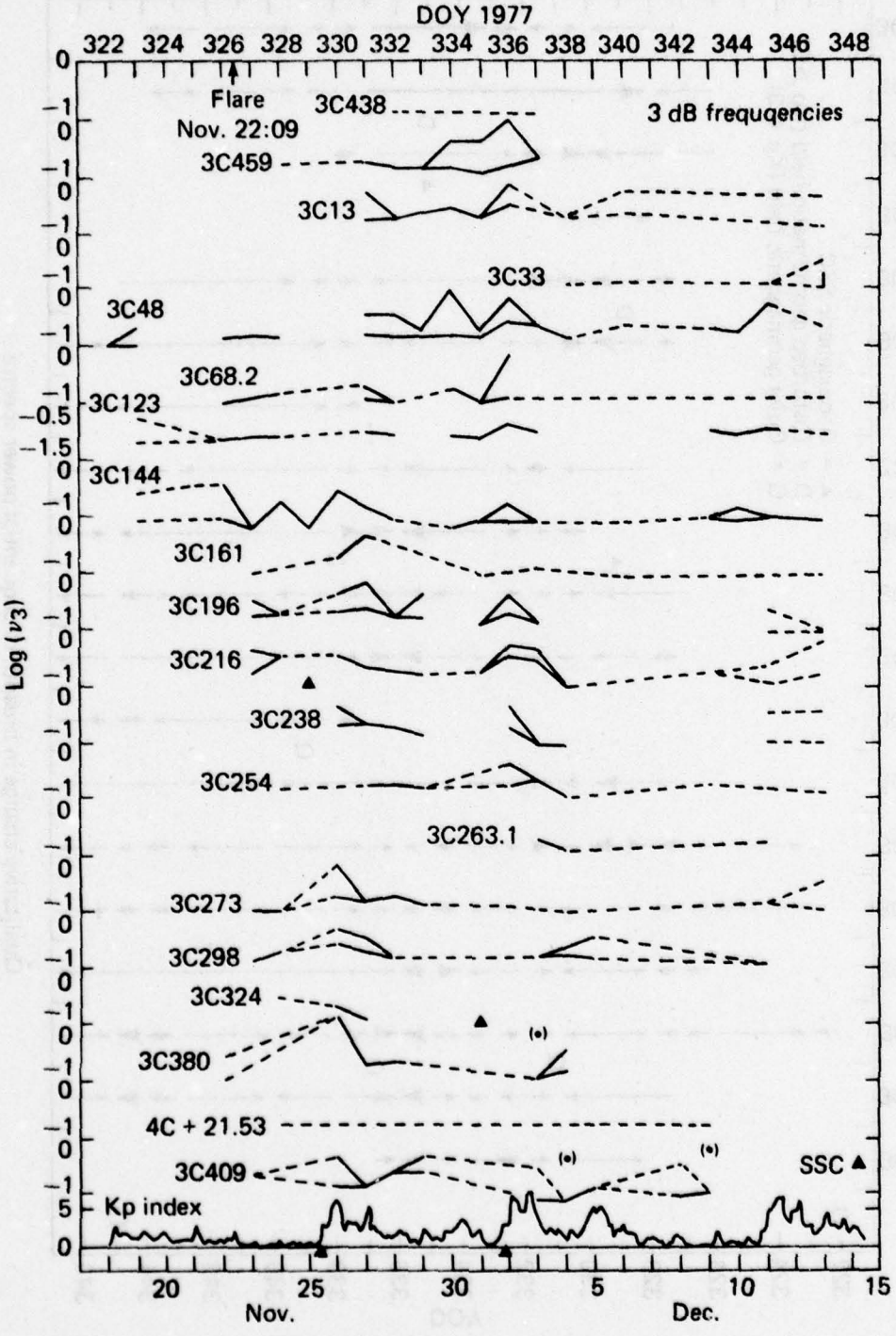
DOY 1977
322 324 326 328 330 332 334 336 338 340 342 344 346 348
Flare
Nov. 22:09
3C438
3 dB frequqencies
3C459
3C13
3C33
3C48
3C68.2
3C123
3C144
3C161
3C196
3C216
3C238
3C254
3C263.1
3C273
3C298
3C324
3C380
4C + 21.53
3C409
SSC
Kp index
Log (ν3)
20 25 30 5 10 15
Nov.
Dec.

FIGURE 4

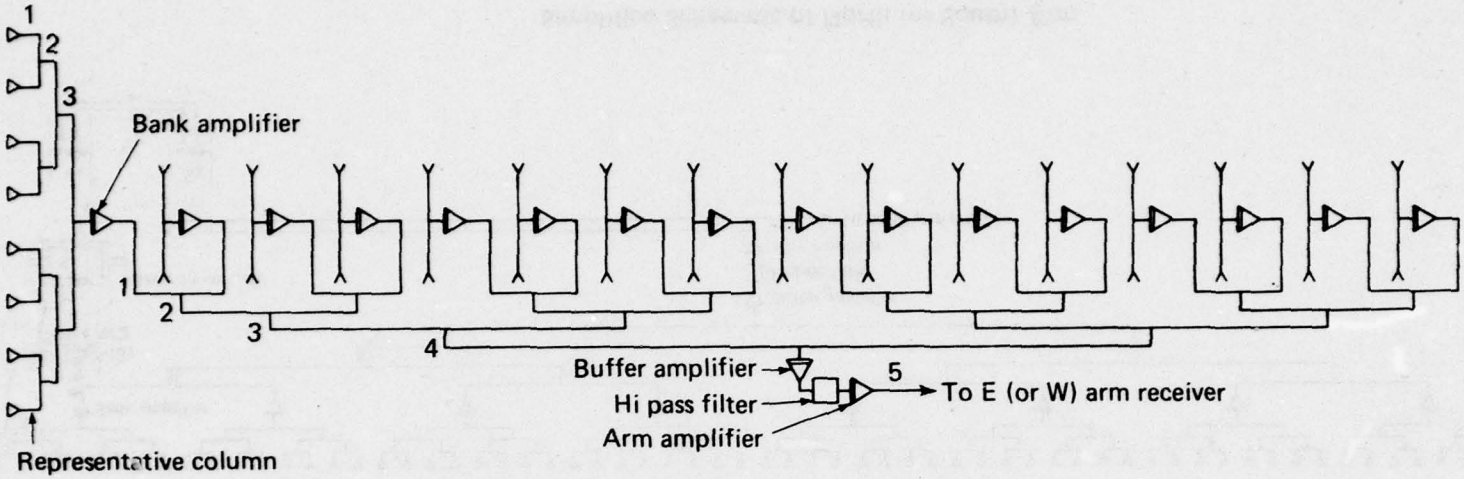

Simplified Schematic of East (or West) Arm

FIGURE 5

THE JOHNS HOPKINS UNIVERSITY
APPLIED PHYSICS LABORATORY
LAUREL, MARYLAND

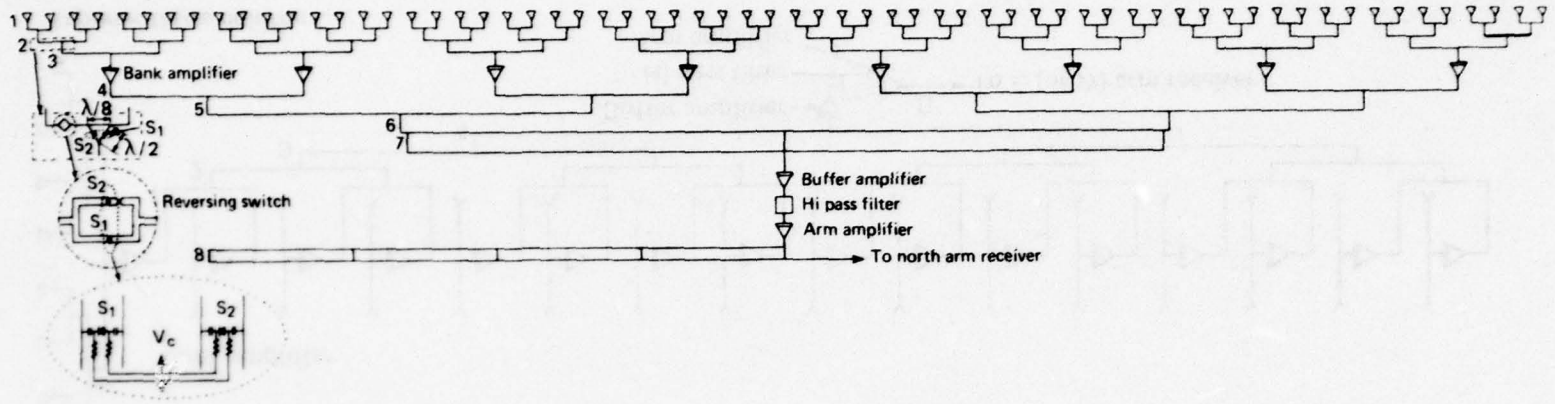

Simplified Schematic of North (or South) Arm

FIGURE 6

FIGURE 7

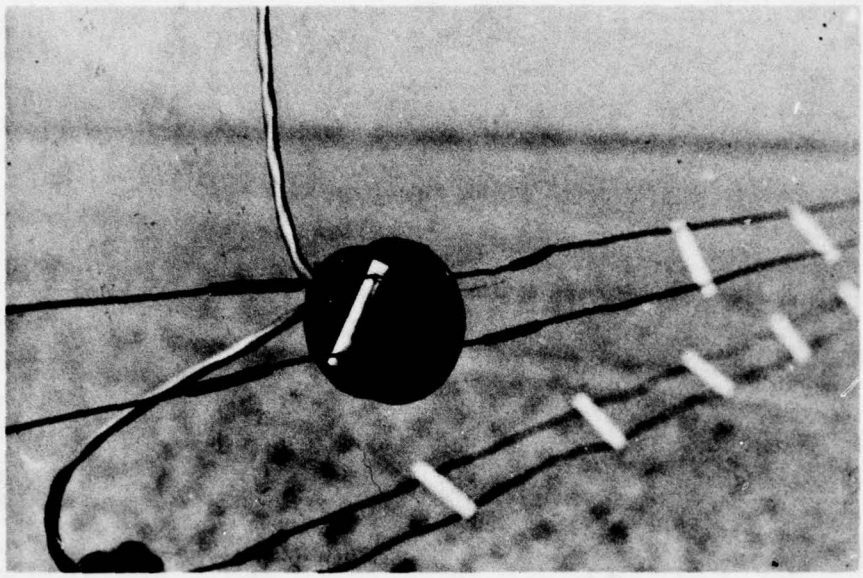

FIGURE 8 *New switch. Components are totally encapsulated in opaque epoxy. Switch leads are protected inside cable jacket.*

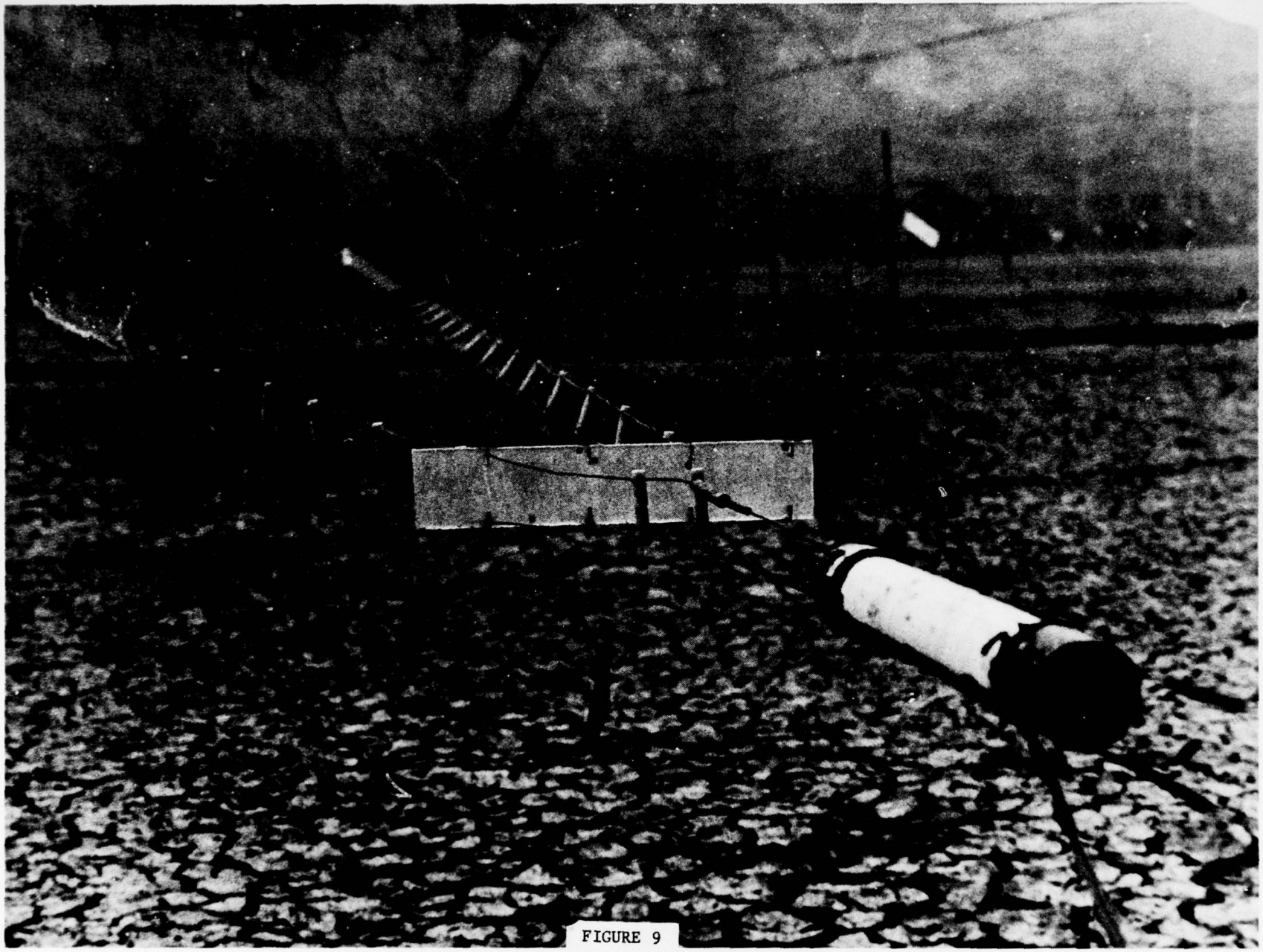

FIGURE 9

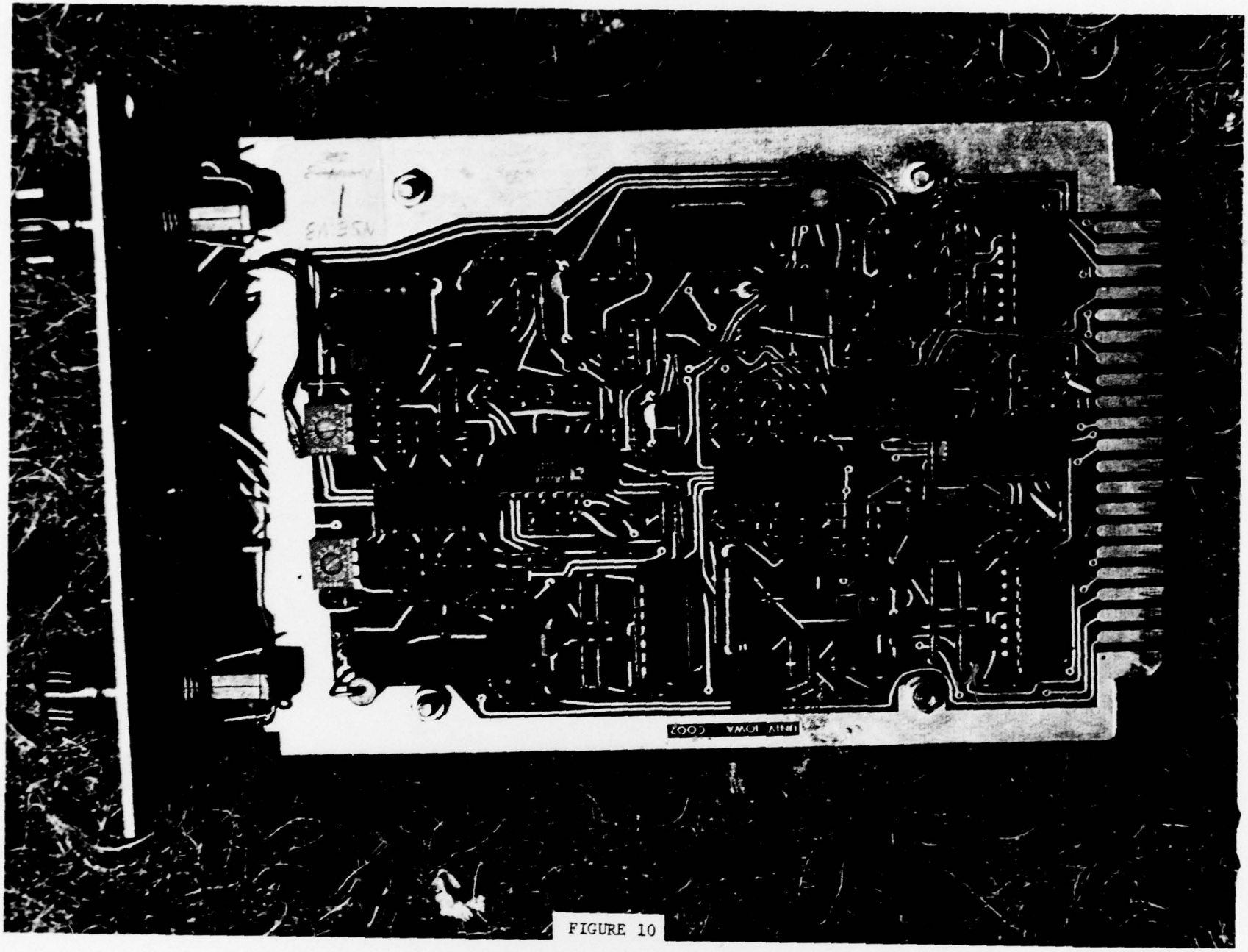

FIGURE 10

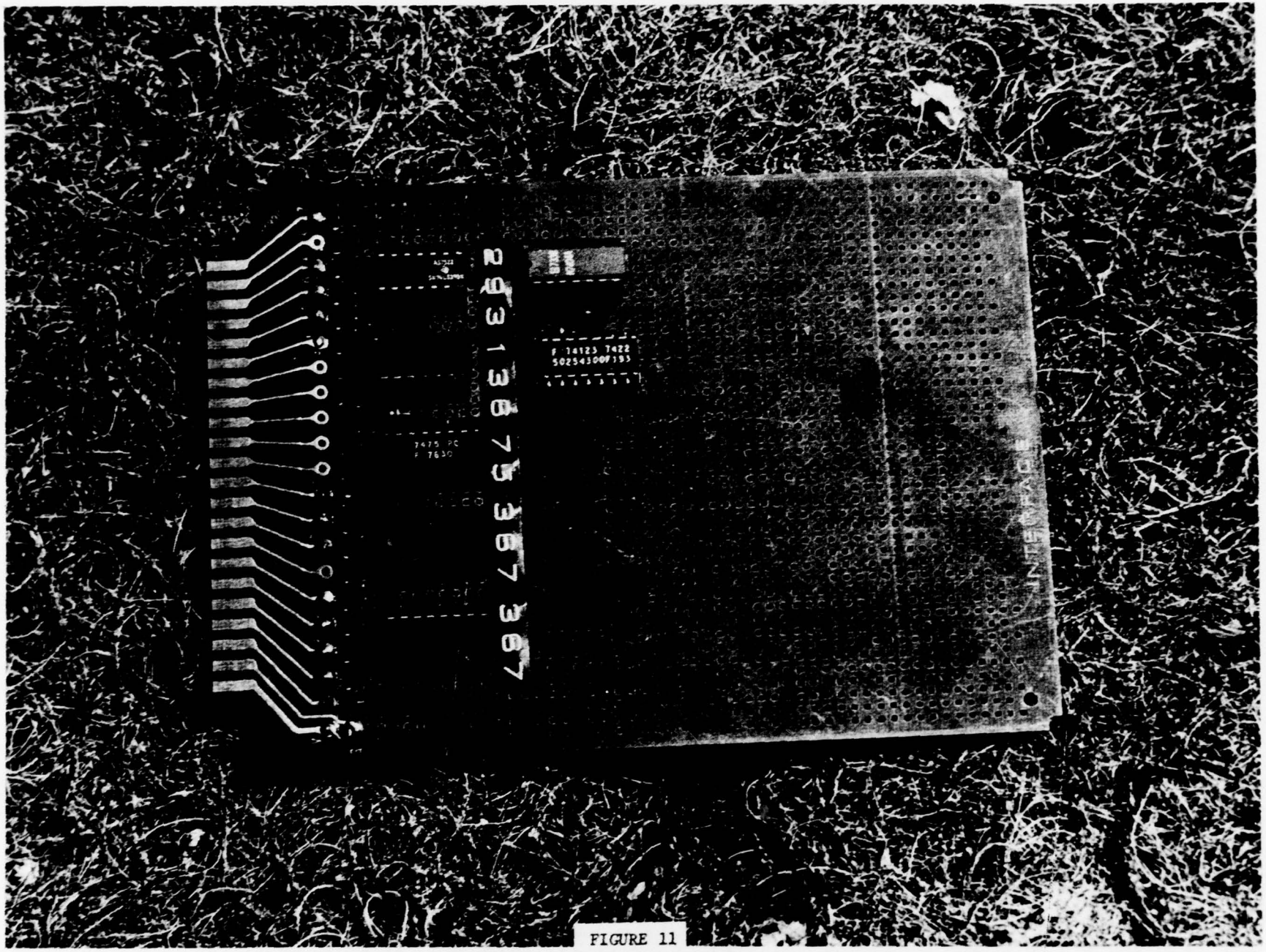

FIGURE 11

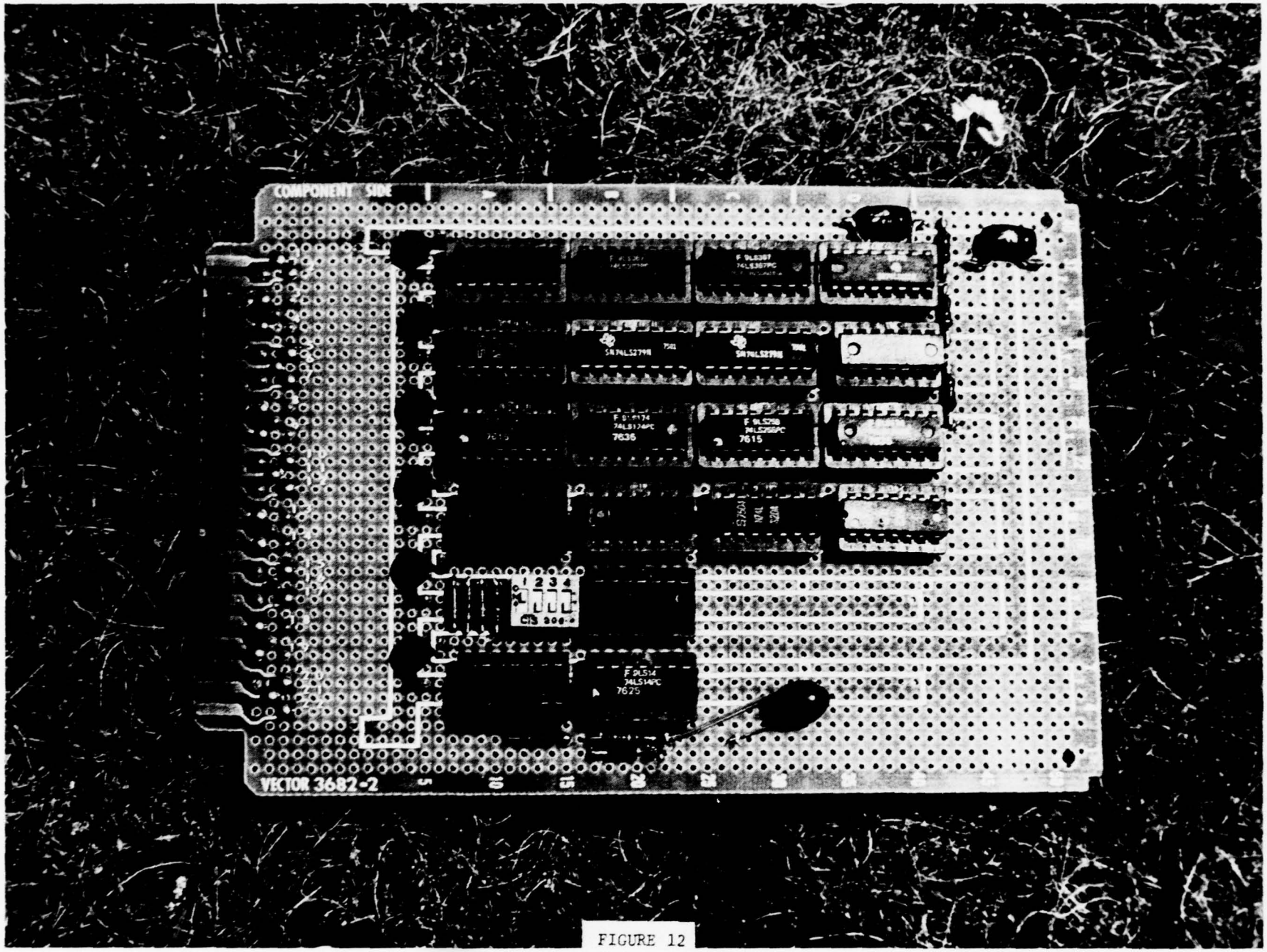

FIGURE 12

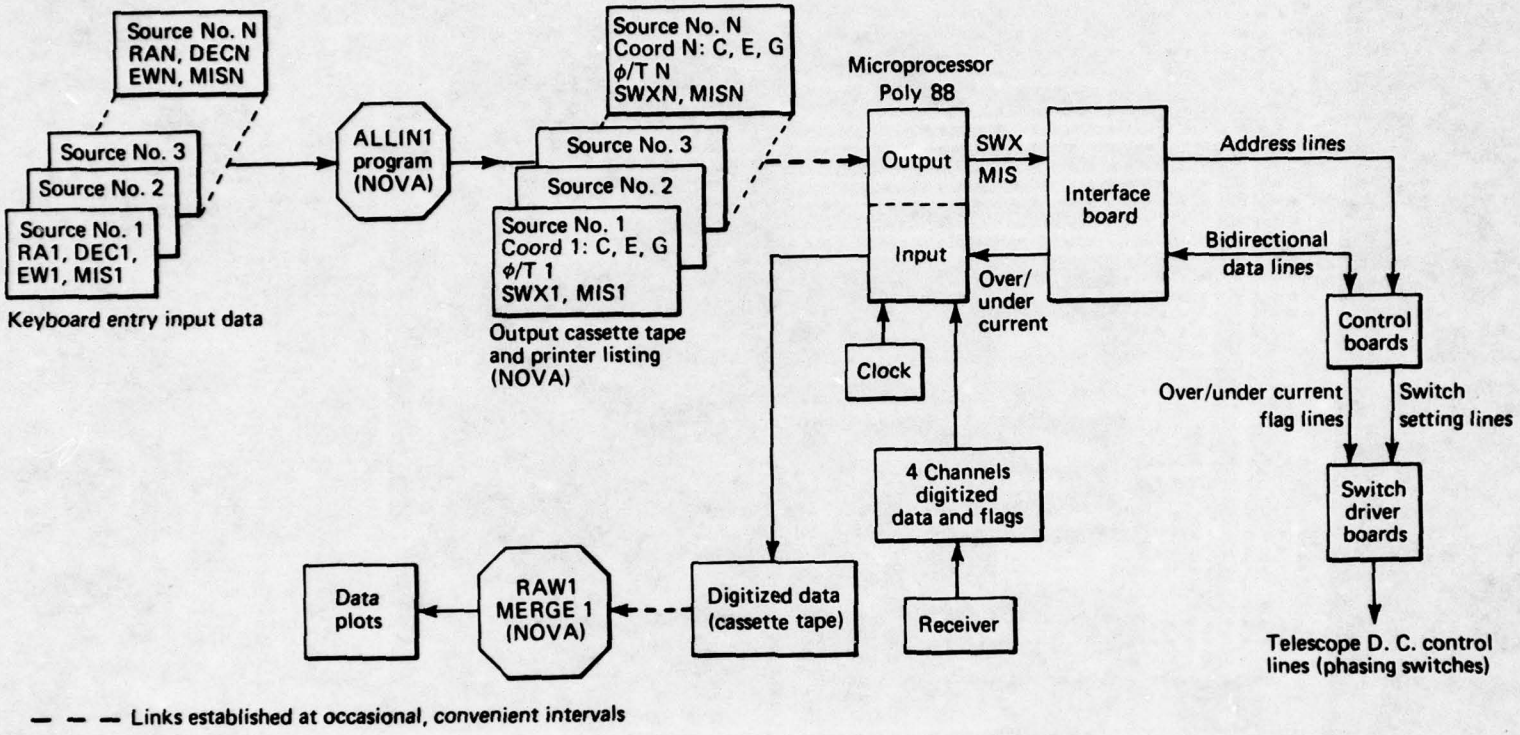
Source No. N
RAN, DECN
EWN, MISN
Source No. 3
Source No. 2
Source No. 1
RA1, DEC1,
EW1, MIS1
Keyboard entry input data
ALLIN1
program
(NOVA)
Source No. N
Coord N: C, E, G
φ/T N
SWXN, MISN
Source No. 3
Source No. 2
Source No. 1
Coord 1: C, E, G
φ/T 1
SWX1, MIS1
Output cassette tape
and printer listing
(NOVA)
Microprocessor
Poly 88
Output
Input
SWX
MIS
Over/
under
current
Interface
board
Address lines
Bidirectional
data lines
Control
boards
Clock
Over/under current
flag lines
Switch
setting lines
4 Channels
digitized
data and flags
Switch
driver
boards
Data
plots
RAW1
MERGE 1
(NOVA)
Digitized data
(cassette tape)
Receiver
Telescope D. C. control
lines (phasing switches)
— — — Links established at occasional, convenient intervals

FIGURE 13

APPENDIX A

April 1977

PREDICTION OF SOLAR PARTICLE EVENTS AND GEOMAGNETIC ACTIVITY USING INTERPLANETARY SCINTILLATION OBSERVATIONS FROM THE IOWA COCOA-CROSS RADIO TELESCOPE

Interim Scientific Report Covering the Period 1 April 1976 – 31 March 1977, on Contract NPP-75-157, Air Force Office of Scientific Research

E. C. Roelof, Principal Investigator
B. L. Gotwols, Co-Investigator
D. G. Mitchell
Johns Hopkins University Applied Physics Laboratory

W. M. Cronyn, Co-Investigator
S. D. Shawhan, Co-Investigator
University of Iowa

THE JOHNS HOPKINS UNIVERSITY ■ APPLIED PHYSICS LABORATORY
Johns Hopkins Road, Laurel, Maryland 20810

1. INTRODUCTION

This interim scientific report covers the first year (1 April 1976 - 31 March 1977) of the research conducted under AFOSR contract NPP-75-157 "Prediction of Solar Particle Events and Geomagnetic Activity Using Interplanetary Scintillation Observations from the Iowa COCOA-Cross Radio Telescope".

In September 1975 a two year program of observations of interplanetary radio wave scintillations aimed at the prediction of solar particle events and geomagnetic activity was proposed to AFOSR. This proposal called for the installation at the Clark Lake Radio Observatory of a digital data acquisition system which would be designed and built at APL. Further it was proposed to evaluate the feasibility of the use of the observations for prediction of solar-terrestrial disturbances.

Observations were taken May-August 1976 at CLRO and reduced and analyzed at the Applied Physics Laboratory. Interplanetary scintillation power spectra were examined, and a significant new prediction signature for approaching solar wind turbulence was identified. This signature, which characterizes the shape of the spectrum, contains more information than the commonly-used scintillation index, which contains the band-passed total power of the spectrum. We intend to pursue the study of spectral signatures as a diagnostic of plasma turbulence approaching the earth. During the summer of 1976, the turbulence detected by spectral analysis was well-associated with geomagnetic disturbances caused by turbulent solar wind streams (measured by spacecraft) impinging on the magnetosphere. The turbulence detection preceded the geomagnetic disturbance by at least one day.

2. SUMMARY OF OPERATIONS: APRIL 1976 - MAY 1977

Our proposal in September 1975 called for the installation at the Clark Lake Radio Observatory of a digital data acquisition system within 6 months after the commencement of funding. In fact the data acquisition was installed in only 1.5 months. This compression in schedule was possible because of the provision by APL of independent research and development funds which allowed construction of the data acquisition system to begin before funds were received from AFOSR.

Observations were conducted continuously on the COCOA-Cross Radio Telescope (34.3 MHz) from mid May 1976 until late August 1976. Of the ~ 150 radio sources observed each day, a subset of 41 sources proved favorable enough in location, flux and angular diameter to produce measureable scintillation power (see Table 1). The sources are shown in ecliptic coordinates in Figure 1. Of these, 15 consistently rendered spectra with sufficient signal-to-noise ratios to be used in the analysis of the scattering in the interplanetary medium. Observations on the COCOA-Cross were supplemented with simultaneous observations at 38 MHz on the University of Maryland TPT array, also at CLRO, using the same data acquisition system. At the conclusion of the observation period it was clear that the data set could be substantially improved by upgrading the array, in order to improve the signal to noise ratio, reduce suseptibility to radio frequency interference, and increase the reliability of the system during adverse weather conditions. This upgrading is discussed more fully in the next section.

Interpretation of the data began in the fall of 1976 and is continuing at present. A brief discussion of our preliminary results is presented in Section 5 and a list of publications in Section 7.

3. INSTRUMENTATION

3.1 Digital Data Acquisition System

A block diagram of the data acquisition system constructed at APL for use in this study is shown in Figure 2. This system allows up to 4 analog signals to be simultaneously digitized and recorded on magnetic tape. A number of optional sample rates are available up to the maximum rate of 10 samples/sec. In addition, each analog channel has an event channel associated with it which allows a single bit of information to be recorded, such as marking the instant when the antenna was phased up for a new source. All timing information is derived from the highly accurate (crystal controlled) serial time code which is supplied from the University of Maryland's time code generator.

Since power spectra are being calculated from the 10 SPS data collected by this system, it is particularly important to minimize the amount of aliasing that occurs above the 5 Hz Nyquist frequency. This is accomplished by placing a low pass filter in front of the analog-to-digital converter. This filter is a 4 pole Chebyshev design with a cutoff frequency of 2.9 Hz, and an attenuation at the Nyquist frequency of 20 dB. This perhaps overly conservative design virtually guarantees freedom from spectral ambiguities due to aliasing.

TABLE 1 — Sources for which scintillation index was routinely calculated

3C13	3C147	3C286
3C33	3C154	3C287
* 3C48	3C161	3C293
3C55	* 3C186	3C295
* 3C68.2	* 3C196	* 3C298
3C79	* 3C216	3C310
3C82	3C225	* 3C380
3C89	3C252	* 4C+21.53
3C103	* 3C254	3C409
3C111	* 3C263.1	3C436
3C123	3C268.4	3C438
3C125	* 3C270.1	3C456
3C134	* 3C273	* 3C459
* 3C144	* 3C280	

* Source for which the power spectrum was frequently calculated.

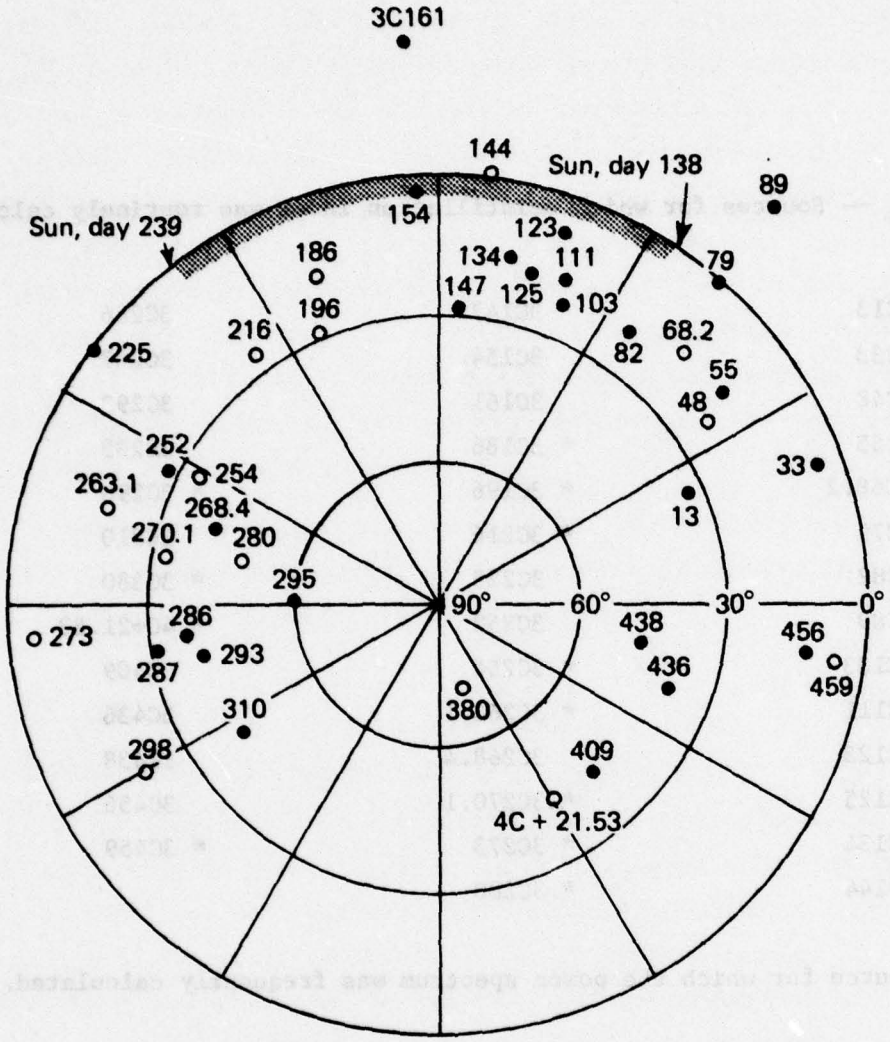

Fig. 1 Subset of 41 sources observed by the COCOA-Cross radio telescope. Sources plotted with an open circle consistently yielded useful spectra.

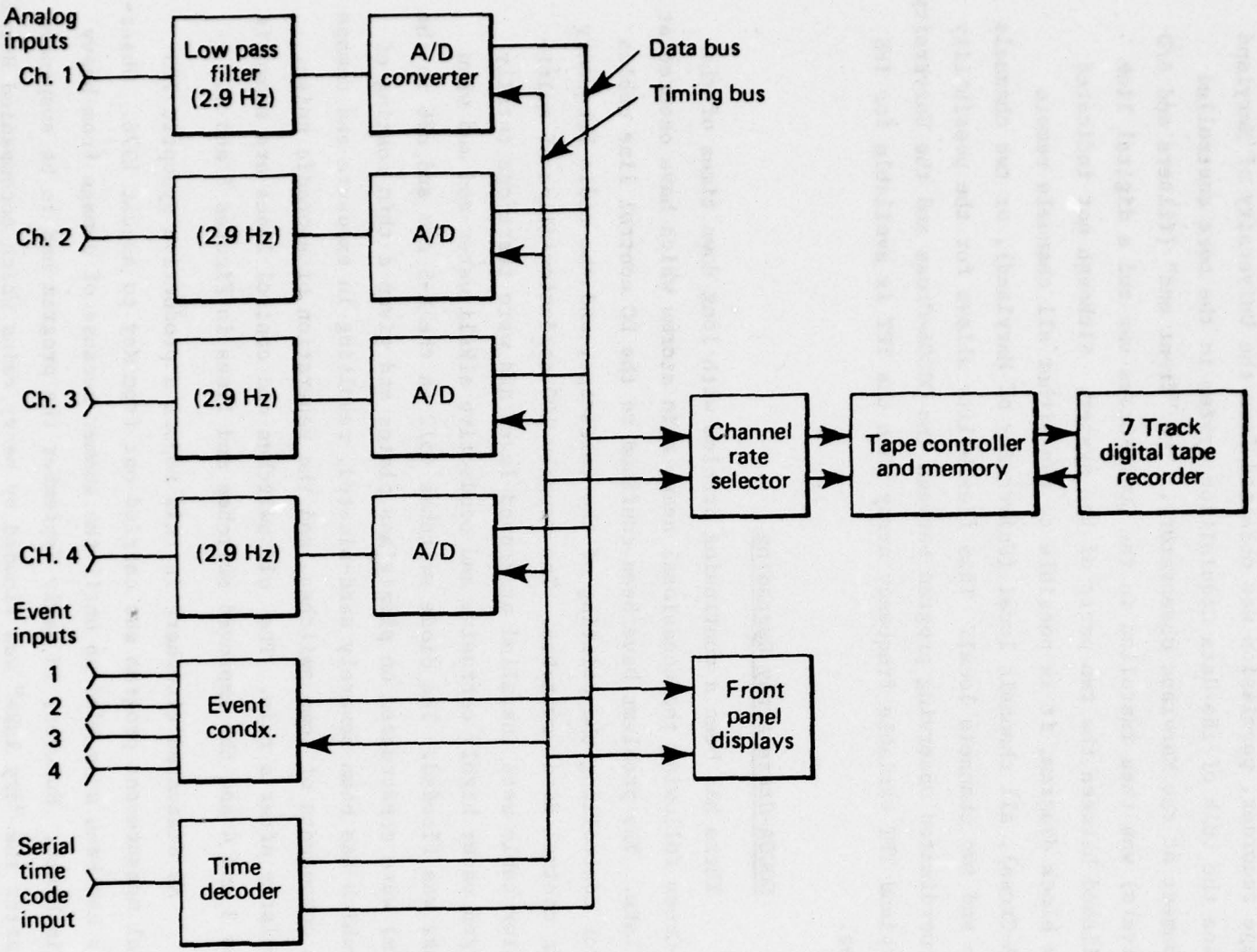

Fig. 2 Block diagram of the data acquisition system used to obtain data from the COCOA-Cross and TPT arrays.

Despite the almost daily occurrence of blowing sand, the COCOA-Cross equipment van is not yet equipped with any particular environmental controls. Since this would lead to a greatly shortened life for the digital tape recorder, permission was obtained from the University of Maryland to place the bulk of the data acquisition system in the more controlled environment of the Maryland observatory. The "front end" (filters and A/D converters) was then installed in the COCOA-Cross van and a digital link established between the two parts of the system. Although not indicated on the block diagram, it is possible to run either all channels remote (COCOA-Cross), all channels local (University of Maryland), or two channels remote and two channels local. This flexibility allows for the possibility of a coordinated observing program between the COCOA-Cross and the University of Maryland TPT variable frequency array when the TPT is available for IPS studies.

3.2 COCOA-Cross Array Upgrading

There has been a continuing problem with long down times of the COCOA-Cross following the occasional heavy rain storms which have occured at Clark Lake. The problems have been confined to the DC control line cables used for controlling the pointing of the telescope, and the radio frequency phasing control diode switches. The roughly 100 conductor-miles of multi-conductor cable were installed at ground level and were therefore totally submerged under highly corrosive and conductive alkali water and mud when the lake was flooded. The diode switches (512 in the N-S arm and 896 in the E-W arm) were constructed on plexiglass plates and given a thin coating of epoxy which has been severely sand-blasted, resulting in exposure and damage to the components of some switches, and the generation of sporadic noise, particularly after a rain. The old switches and control lines are shown in Figures 3 and 4 and the improved switches and lines in Figures 5 and 6.

As discussed elsewhere in this report a productive synoptic IPS spectral measurement program was carried out from May to August 1976. Observations had been suspended up until the summer because of damage from heavy rains in March. However, in early September the program had to be suspended again after the "dry lake" was flooded by heavy rains which accompanied Hurricane Kathleen. In early October, before the lake had dried out enough to

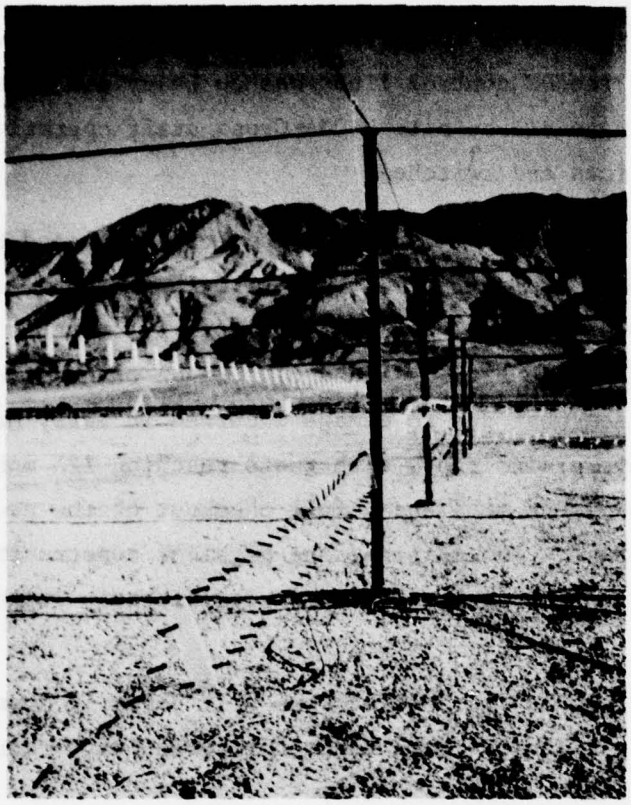

Figure 3 View of E arm column looking North. Note DC control line cables on ground at base of pole.

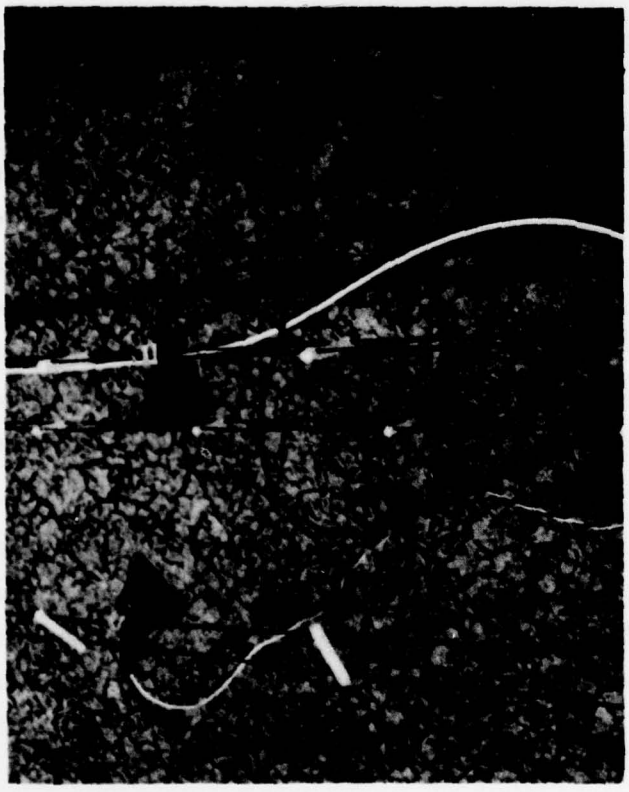

Figure 4 Excellent picture of a pair of old-style switches. Note how visible components are (very thin coating of epoxy) and exposed individual switch wires.

resume observations, the Lake was flooded for a third time in 1976 by heavy rains. The resulting damage to the DC control lines was so heavy and extensive that we decided to concentrate all on-site COCOA-Cross staff operations on replacement of the control lines and switches.

All the multiconductor DC control lines have now been replaced by a network of copperweld open-wire lines which are at least 12 inches above the ground, and all of the 1408 diode switches have been replaced by switches which are totally encapsulated in epoxy (see Figures 5 and 6). Final checkout of the reconfigured array was delayed somewhat due to damage incurred in early March 1977 as the result of a very severe wind storm with gusts reaching 125 mph. At this writing this damage has been corrected and a full checkout of the new control lines and switches is underway. In addition, the physical construction of the array has been strengthened in many areas so as to significantly improve its resistance to wind damage.

It is expected that synoptic IPS observations will begin in June and will no longer be interrupted by extensive down times following heavy rains and very high winds.

4. DATA REDUCTION

All raw data are transcribed from the 7 track tape written at Clark Lake to 9 track tape for study at APL. The main beam response and scintillation power in the 0.1 to 1.5 Hz band are then digitally calculated for each observation and printed on a Versatek printer-plotter (Figure 7). The scintillation index is then calculated as described in Figure 7. These computer generated plots have the great advantage over our former (prior to May 1976) strip-chart type of presentation in that the computer can first scan the entire observation and select the best one of the available standard dynamic ranges for displaying each channel. In this way, the scaling errors of our old scheme, which occurred when the width of the track became comparable to the deflection, have been essentially eliminated.

Examination of the time history plots mentioned above allows rapid identification of sources which are likely to yield useful power spectra. The power spectrum analysis consists of first taking out long-term trends by passing the data through a digital high pass filter (4 pole, matched Z Butterworth design)

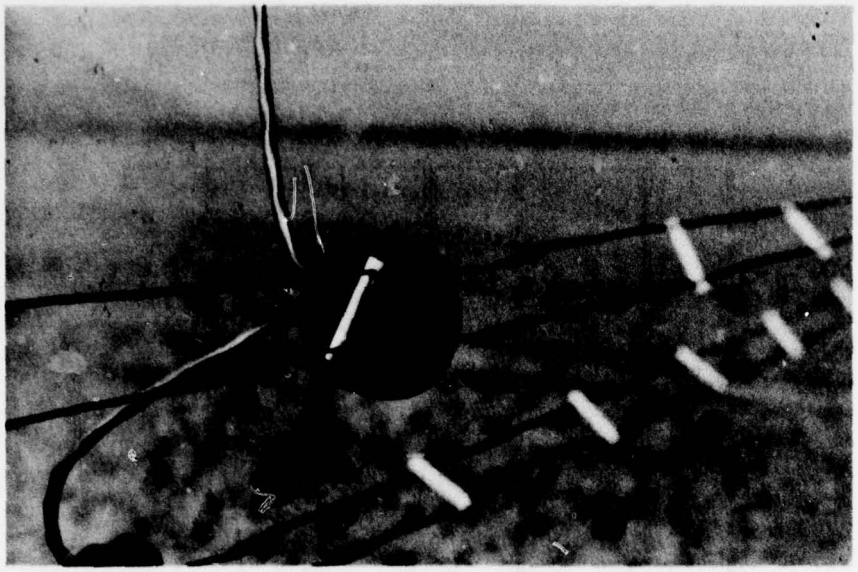

Figure 5 New switch. Components are totally encapsulated in opaque epoxy. Switch leads are protected inside cable jacket.

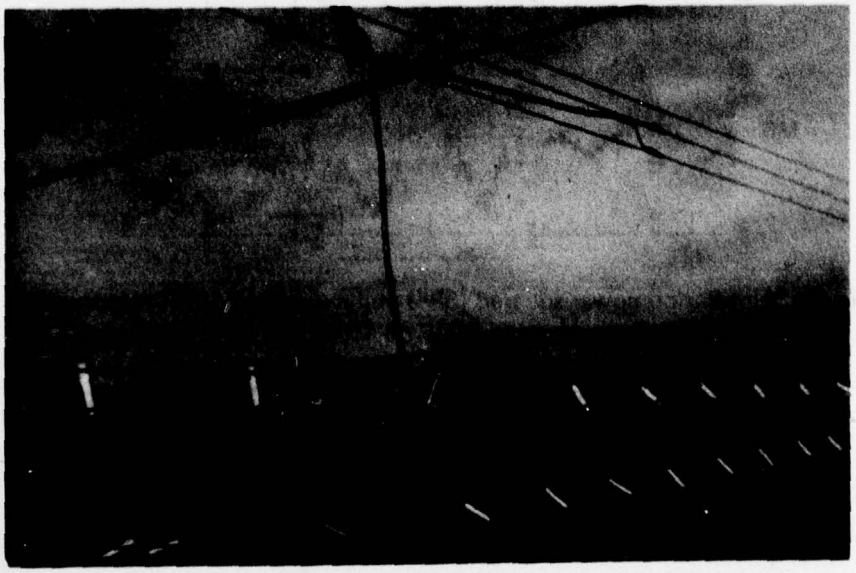

Figure 6 A new switch assembly (description as per Figure 5). DC control lines are elevated far above any possible water level and are open so that there are no cable joints which require sealing.

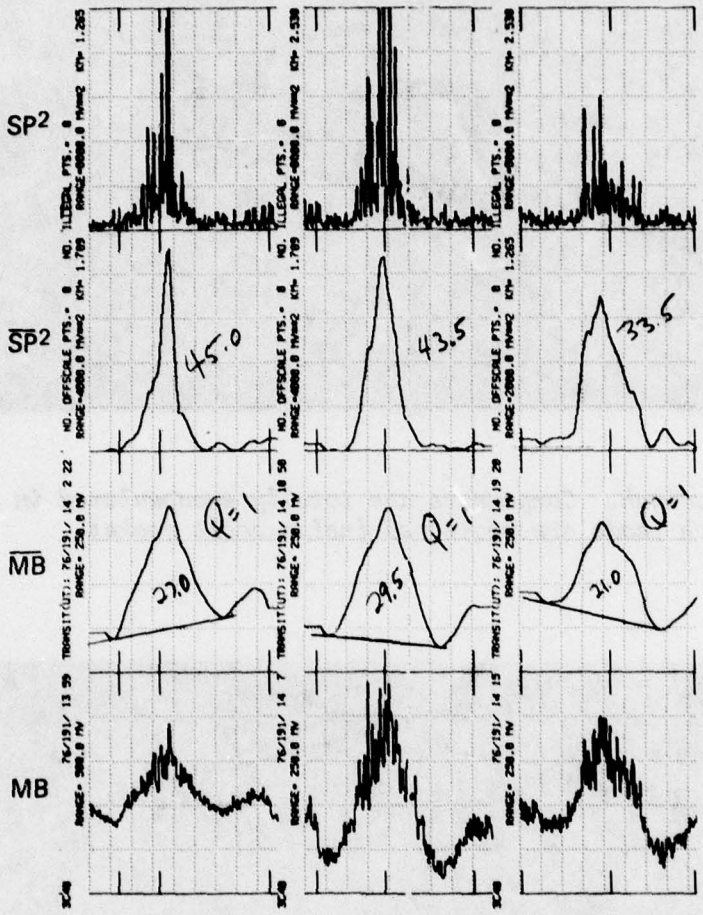

Fig. 7 Scintillation power squared (SP^2) and main beam (MB) response for three successive transits of 3C48 on 1976, day 191. Unbarred variables are 2.5 second averages which are plotted chiefly to aid in the identification of interference. Barred variables are 50 second triangle weighted averages which are scaled by hand (in minor chart divisions) and then combined with the scale factor (KM) just to the left of each SP^2 curve to yield the scintillation index. For example, for the leftmost set of curves the scintillation index is: $m = 1.789 \cdot (\sqrt{45.0})/27.0 = 0.44$. The Q values shown are quality factors which are helpful when summarizing a large number of observations.

with a cutoff frequency of 0.02 Hz. These highpass data are then broken into 256 point segments (25.6 sec) and a fast Fourier transform is performed on each segment. The average magnitude squared of each Fourier component is then calculated and corresponding components from each 256 point transform are added together to give the desired spectral estimates. On those sources which are observed more than once per day all of the spectral estimates are further combined into one composite spectral estimate with improved stability (Figure 8). In order to further increase the statistical stability of the spectral estimates, the spectra are smoothed with a Hanning spectral window. This technique is equivalent to a combination of Bartlett and Hanning smoothing. For example, for the spectrum shown in Figure 8, which represents 9 minutes of data, there are 112 degrees of freedom.

Two curves are plotted in Figure 8. The upper curve is the raw uncorrected spectrum which consists of a scintillation component plus a white noise component due to system noise. The sharp cut-off above 3 Hz is due to an anti-aliasing filter. Since in our observations the scintillation component of the spectrum has always been found to be negligible above 2 Hz, we estimate the white noise amplitude by averaging across the 2 to 3 Hz range and subtract that estimate from each of the spectral points. This yields the lower curve which for convenience has been renormalized. The low frequency droop below about 0.04 Hz is due to the digital high-pass filter.

Three empirical parameters are tabulated from each of the many spectra examined. These are: ν_3 and ν_6, the frequency at which the corrected spectrum falls 3 and 6 dB respectively below the low frequency plateau, and α, the high frequency slope of the power law. The frequencies ν_3 and ν_6 are not taken directly from the spectral points but instead are read from an eye estimate of the best fitting curve to the data points.

5. DATA ANALYSIS

The reduced data were analyzed using comparisons with models of interplanetary scintillation and applied to a study of the feasibility of using them for the prediction of possible geomagnetic activity resulting from the interaction of the earth's magnetosphere with solar wind disturbances. Displaying the spectra on a log-log plot (example, Figure 8), they typically displayed a

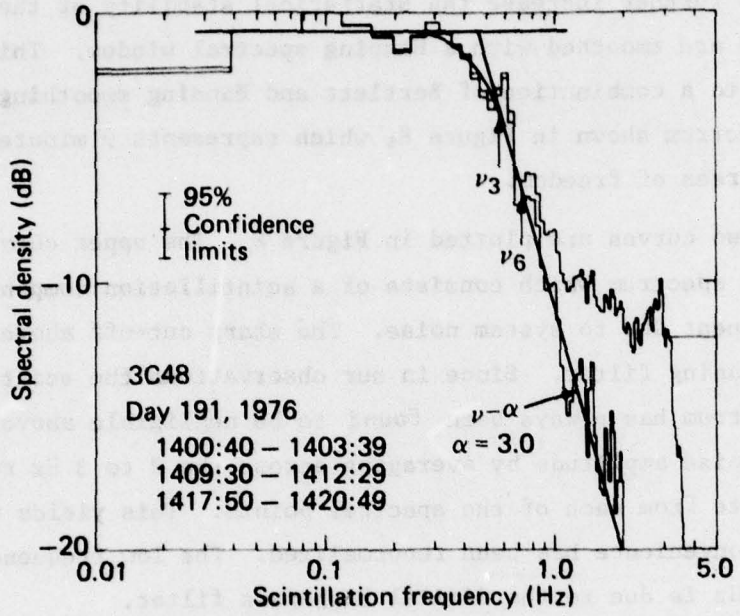

Fig. 8 Power spectrum of the scintillating radio source 3C48 on 1976, day 191.

flat plateau from very low frequencies to a turn-over into a nominal power-law slope, the turn-over occurring at anywhere from less than 0.1 Hz up to 0.5 Hz. Both the frequency and the rate at which the spectrum turns over into the power law provide information about the velocity of the scattering medium and its density turbulence profile. The slope of the power-law also provides information about the turbulence profile. Therefore, the spectra are parametrized by recording the power-law slope (α), the frequency at which it drops to 3 dB below the plateau (ν_3), and the frequency at which it drops to 6 dB below the plateau (ν_6). These three parameters then serve as useful characterizations of the spectra for the analysis of large amounts of data.

A plot of ν_3 versus time (Figure 9) for the 15 sources on which we had reasonable continuity demonstrates the utility of this sort of analysis for the prediction of the arrival at earth of solar wind disturbances. The days on which solar wind stream-stream interaction regions arrived at the earth, as determined from IMP-7 and 8 spacecraft data, Figure 10, are indicated in Figure 9, and shaded on the figure about those sources which were located favorably for prediction. The most useful source during this observation period for the purpose of predicting the arrival of disturbances was 3C273. It lies to the east of the sun, from which direction corotating disturbances come, and it is at a large enough elongation angle so that it is not in strong scattering. It also lies virtually in the ecliptic plane so that disturbances confined to low solar latitudes lie in the line of sight, unlike the case with higher latitude sources such as 3C263.1 and 3C270.1.

The two events for which we have the best coverage are day 182 and day 197. In each of these cases, the spectra on 3C273 displayed increases in ν_3 (broadening in the spectra) at least 1 day before the arrival of the disturbance at earth. This increase in ν_3 is what one would expect on the basis of modelling of the scattering in the medium, as a turbulent region moves closer to the earth. A close-up study of the geometry and the power spectrum for 3C273 leading up to the geomagnetic activity on day 197 is shown in Figure 11. In addition, the day 197 event appears to have been seen by other eastern sources (3C270.1, 3C298), indicating that the turbulent region extended above the ecliptic plane in the north. Unfortunately, 3C216 and

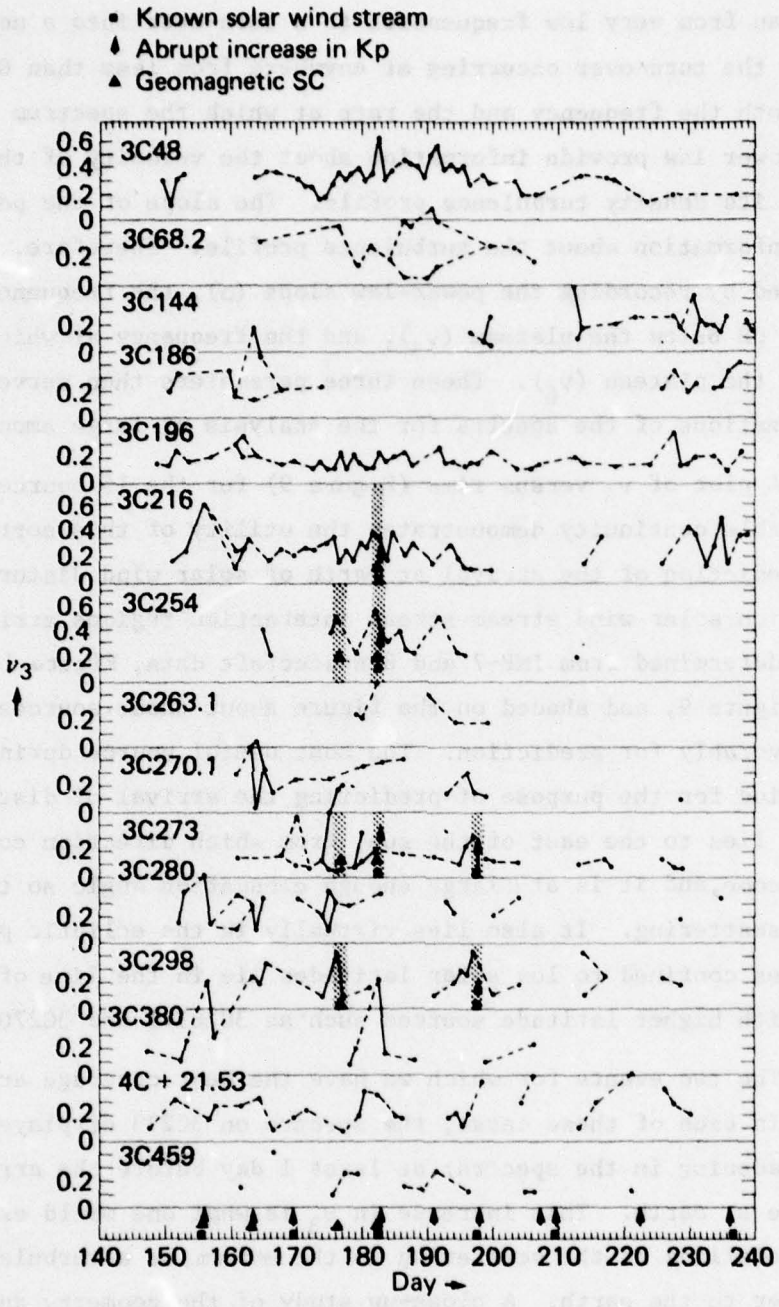

Fig. 9 ν_3 **versus time for 15 sources – known solar wind streams, SC's and abrupt increases in** K_p **index are indicated. The symbols are repeated (shaded) to point out the areas in the data consistent with prediction of events. On those spectra displaying two plateaus both values of** ν_3 **are plotted.**

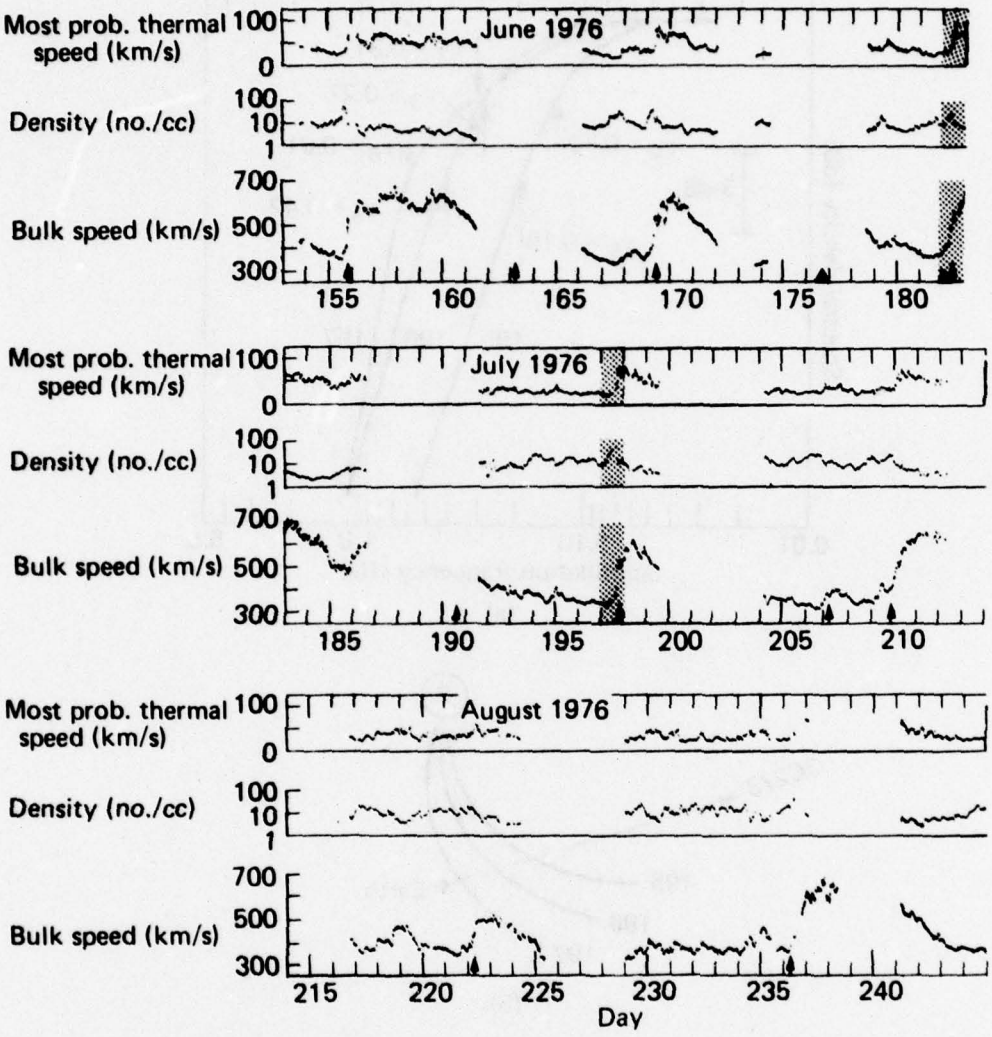

Fig. 10 Solar wind probe data (*Lazarus, Solar-Geophysical Data, 1977*), days 153-244, showing recurring corotating solar wind streams. Shaded areas correspond to known streams with sufficient IPS data coverage to be used in the prediction study. Triangles are geomagnetic sudden commencements; arrows are abrupt increases in K_p index.

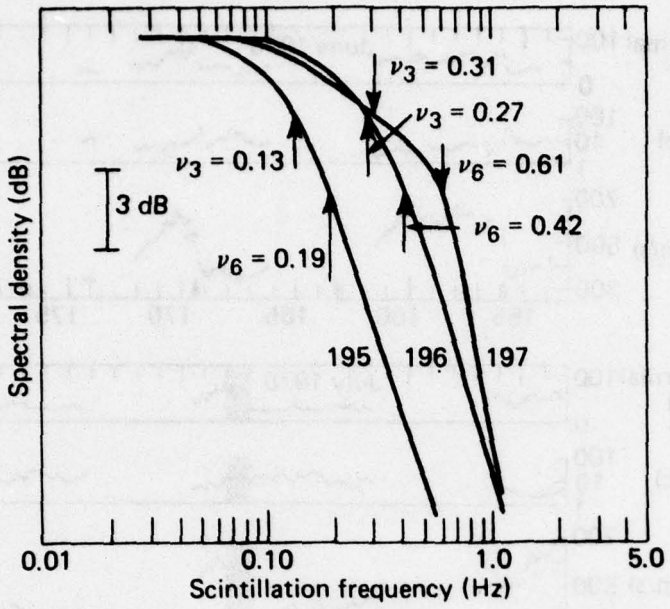

Fig. 11 (a) Smoothed scintillation spectra for 3C273 on days 195, 196 and 197 illustrating progressive broadening as a corotating region approaches the earth.
(b) Line of sight to 3C273 projected onto the ecliptic plane on 1976, day 197. Also shown is the approximate shape of the center of a corotating density enhancement for days 195, 196 and 197 at the time when 3C273 was observed.

3C196 are both at elongations small enough to be in strong scattering, for which the present prediction analysis is not well suited.

Another aspect of the data analysis is shown in Figure 12. These are scatter plots of ν_3 versus ν_6 (measured on the same spectrum), which give an indication of the rate at which the spectrum turns over into a power-law. The degree to which the points follow a straight line indicates the constancy of the ratio ν_3/ν_6, and the plots show that to a good approximation the spectra represent universal curves whose locus is shifted back and forth in frequency by conditions in the scattering medium.

Figure 13 is a display of scintillation index (m) versus time for several eastern sources, and there is no apparent trend in the data (including that for 3C273) which could be exploited for the purpose of prediction. It is possible that this data might hold more value for prediction in future observations with the improvements currently being made on the instrument.

6. PRELIMINARY EVALUATION AND FUTURE PLANS

We have demonstrated that spectral analysis of interplanetary scintillations enhances their utility as a probe of the interplanetary medium in predicting the arrival of solar wind disturbances at earth, provided that many sources are monitored to the east of the sun. High-speed data collection and reduction to spectra is therefore a highly desirable step in the process of prediction. Our greatest obstacle in the evaluation of this spectral technique has been data gaps and uncertainties in the data due to variable array response. With the improvements and upgrading the array is currently undergoing we anticipate a more definitive evaluation ensuing from another period of data collection. Another way in which we hope to improve the statistics and reliability of the data is by exploiting more fully the 3-beam east-west steering capabilities of the array, in order to spend more time per day on a given radio source. This has already been shown to significantly improve the statistics on a given day's observation of a source during the summer of 1976 observing period. It not only increases the total amount of data going into a spectrum, but decreases the probability of missing a source entirely due to RFI.

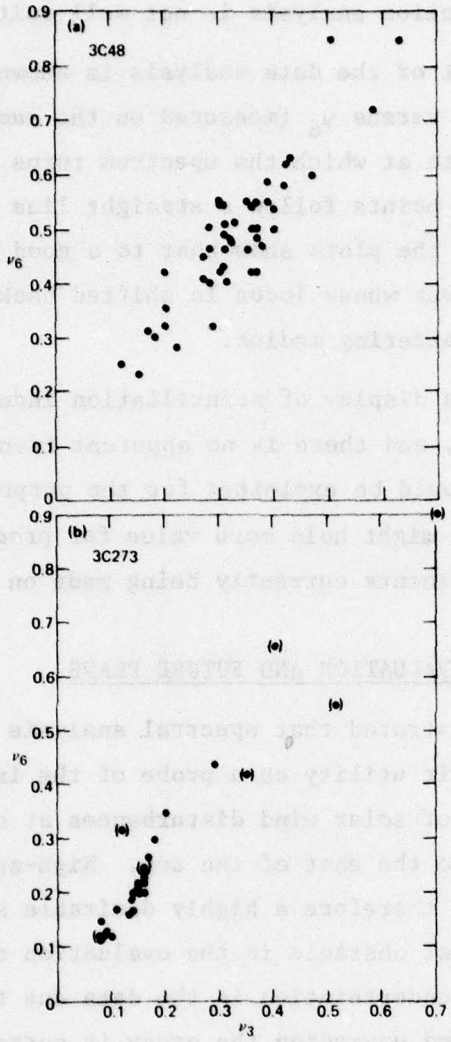

Fig. 12 Scatter plots of ν_3 versus ν_6 for 3C48(a) and 3C273(b). The high correlation between thses two parameters implies a consistently similar shape for the spectra, i.e., a universal curve which shifts on the frequency axis in response to solar wind velocity and turbulence profile. The closer grouping of the 3C273 points may be due in part to large source angular diameter effects. The points in parenthesis for 3C273 are taken from 2 component spectra, which result from two widely separated scattering regions in the interplanetary medium.

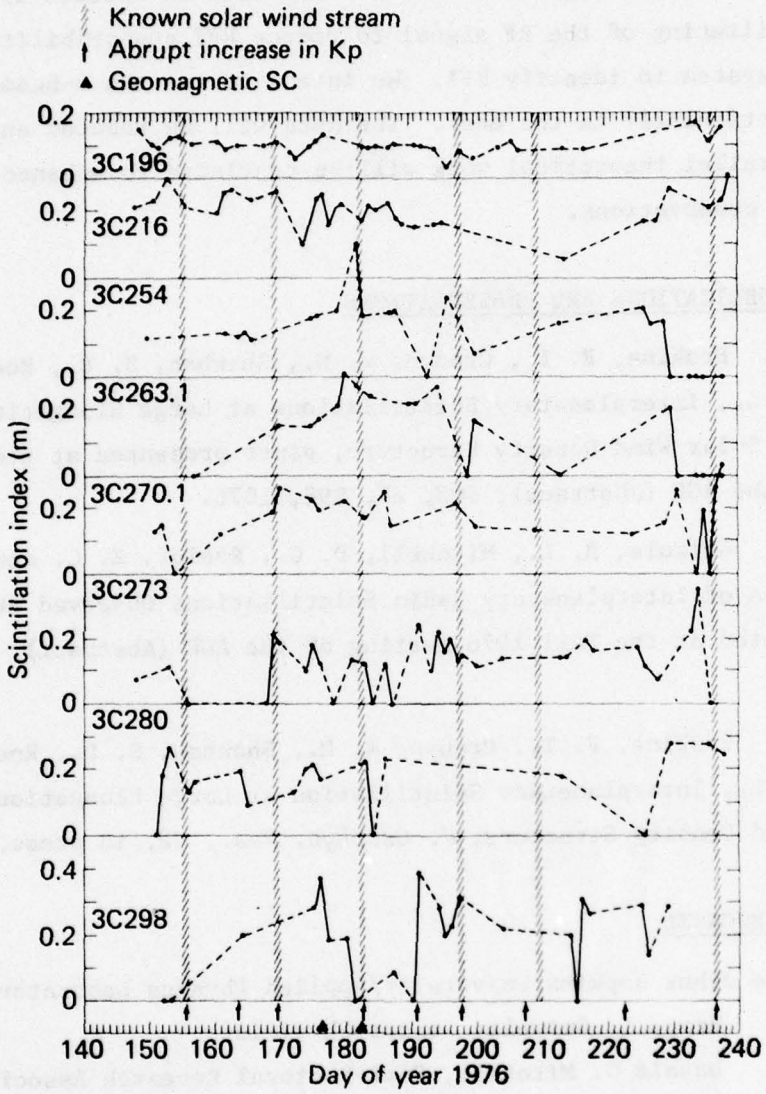

Fig. 13 Scintillation index versus time for 8 eastern sources. The shaded regions indicate the density enhancements preceeding several high speed solar wind streams. Abrupt increases in K_p and geomagnetic sudden commencements are also indicated.

Based on the results we've obtained to date, we have decided to begin synoptic observations again in June (1977) with the upgraded array. Included in the upgrading (besides that discussed in Section 3) will be high-pass filtering of the RF signal to reduce RFI suseptibility, and a better monitoring system to identify RFI. We intend to use the 3-beam per source feature, particularly in the east. The data will be reduced and analyzed at APL, and parallel theoretical work will be continued to enhance our understanding in the observations.

7. PUBLICATIONS AND PRESENTATIONS

1. Erskine, F. T., Cronyn, W. M., Shawhan, S. D., Roelof, E. C. and Gotwols, B. L., Interplanetary Scintillations at Large Elongation Angles: Response to Solar Wind Density Structure, paper presented at the Fall 1976 meeting of the AGU (Abstract), *EOS, 57*, 998, 1976.

2. Gotwols, B. L., Mitchell, D. G., Roelof, E. C. and Cronyn, W. M., Power Spectra of Interplanetary Radio Scintillations Observed at 34.3 MHz, paper presented at the Fall 1976 meeting of the AGU (Abstract), *EOS, 57*, 999, 1976.

3. Erskine, F. T., Cronyn, W. M., Shawhan, S. D., Roelof, E. C. and Gotwols, B. L., Interplanetary Scintillation at Large Elongation Angles: Response to Solar Wind Density Structure, *J. Geophys. Res., 82*, in press, 1977.

8. PERSONNEL

The Johns Hopkins University/Applied Physics Laboratory

Bruce L. Gotwols, Senior Physicist

Donald G. Mitchell, Post-Doctoral Research Associate(1)

Edmond C. Roelof, Senior Physicist

The University of Iowa

Willard M. Cronyn, Assistant Research Scientist

Frederick T. Erskine, Doctoral Candidate(2)

Stanley D. Shawhan, Associate Professor

(1) Research Associate, University of Iowa after 1 February 1977

(2) PhD Physics granted September 1976. Current address: Department of Astronomy, Villanova University, Villanova, Pa.

APPENDIX B

ADDITIONAL SCIENTIFIC RESULTS FROM 1976 OBSERVATIONS

(Condensed from Mitchell, 1978a,b)

In an earlier paper *(Mitchell and Roelof, 1976)* we presented some calculations of intensity spectra, based upon simple assumptions. The electron density fluctuation spectrum was assumed to have the form

$$F(k) = F_o(k_o^2 + k^2)^{-q/2} \exp(-k^2/k_i^2)$$

It was assumed that the outer scale ($2\pi/k_o$) was very much larger than the first Fresnel zone radius ($\sqrt{\lambda L}$, where λ is observing wavelength and L the distance from the observer to the scattering medium), and that the inner scale ($2\pi/k_i$) was near zero. Thus the inner and outer scales have negligible effects on the intensity scintillation spectrum, except for the dependence of F_o on k_o for $q > 3$, or on k_i for $q < 3$. It was further assumed that $F_o \propto r^{-4}$, where r is heliocentric radius. This is reasonably close, but not identical to assuming $< \delta N^2 >^{\frac{1}{2}} \propto r^{-2}$ for an extended medium.

In order to model the scattering from an extended region, we first divide the medium into twenty slabs along the line of sight, each of which contributes roughly equally to the scintillation index of a point source. Thin-screen spectra are calculated for the middle of each slab, and then summed discretely through the medium to produce the extended medium spectrum. Besides the entire medium case (twenty slabs), other cases discussed in this report include models where the scattering occurs only in the first seven slabs closest to the earth, the first thirteen slabs, or a middle range (seven to thirteen). These approximations are more realistic than a single thin screen model in allowing some distribution to the turbulence.

Figure B1 addresses the additional effect of source size on the distance dependence of the scintillation response. The figure illustrates the relative contribution (dm/dL) to the scintillation index (m) as a

function of distance (L) along the line of sight normalized to its maximum value, for different elongations and source sizes. The locations of slabs 7, 13, 19 and 20 are indicated. It can be seen that for large angular diameters, the distant medium contributes little or nothing to the scintillation, thus limiting the distance to which the scintillation is sensitive as a probe of the medium. In modeling the scattering using less than the entire medium, the contribution to the index will go as these curves do within the slabs used and will equal zero outside of these slabs. This approximation is quite reasonable when one considers that the density (and presumably the turbulence) enhancement associated with stream-stream interaction regions is routinely only an order of magnitude above quiescent levels, and the scattering power goes as $< \delta N^2 >$.

There are several parameters which characterize the medium and the radio source. The solar wind velocity (V) is assumed constant and radial. The electron density fluctuations are assumed to have a power-law spatial spectrum. See *Mitchell and Roelof, 1976* for a complete discussion of the computations based on this spectrum and of this technique. The medium irregularities are assumed isotropic, and the source is modelled as having an isotropic Gaussian brightness distribution with an e-folding diameter θ.

We further ignore receiver bandwidth effects and limit the treatment to an observing wavelength of 8.75 meters. This corresponds to the observing frequency (34.3 MHz, 500 KHz bandwidth) of the University of Iowa COCOA-Cross radio telescope.

The most easily obtained spectral parameters are the apparent high frequency slope (α) and the turnover frequency (ν_3) defined as the frequency at which the spectrum drops to 3 dB below the Fresnel plateau. The Fresnel plateau is the flat portion of the spectrum at low frequencies and is defined operationally by drawing a straight line through the low frequency points between $\sim$ 0.08 Hz and the point at which a smooth curve drawn through the spectrum falls off monotonically. A more complete description of the experimental techniques employed are available in *Gotwols et al., 1978.*

As the errors inherent in α are greater than those in ν_3 and the need for accuracy for physical interpretation greater in α than in ν_3 (α has a smaller relative dynamic range than ν_3), we will be primarily concerned with the direct comparison of ν_3 with the model and will use α only as a rough indicator of consistency between the model and the data.

For small sources ($\theta \leq 2''$) whose spectrum is dominated by Fresnel turnover, ν_3 is by the nature of its definition biased toward the more distant medium. This is because any contribution from the distant medium just adds power at low fluctuation frequencies.

However, for larger source sizes ($\geq 3''$) the scattering from the most distant medium is severely attenuated, and so the scattering region is in effect more localized. In this case ν_3 becomes a better indicator of the distance to the scattering medium. In the limit of very large sources ($\geq 5''$), the dominant scattering region is near earth (≤ 0.3 AU). In this case the cut-off of the spectrum is source size dominated.

We display ranges of ν_3 from theoretical spectra at a range of elongations ($60° \leq \epsilon \leq 120°$) in Figure B2, with source size as a parameter. It should be emphasized that for each realization of the medium employed here (with the exception of the entire medium case), a change in elongation angle of twenty degrees also represents a sizeable change in the shape of the density profile, for a fixed choice of slab numbers. For example, slabs 1-7 are of different thicknesses and distances at different elongations. In these idealized cases, the variation in elongation can be looked upon as a change in the medium profile. In fact, for these large elongation angles, the daily variability in the turbulence profile dominates real elongation trends in the profile. Thus in comparing an observation at a given elongation with a ν_3 calculated for the proper source size, one would not necessarily expect to find a fit to the theoretical ν_3 at the same elongation, unless one closely approximated the actual turbulence and velocity profiles. However, even with the limited resolution of the ranges of ν_3 calculated in Figure B2, one can roughly infer source size and the configuration of the medium by comparing a sufficient sampling of experimental data with these ranges. Note that for each realization of the medium there is a decreasing progression of ν_3 with increasing source

size. Thus two sources of different sizes observed at the same time at the same elongation would be separated by this dependence. By comparing model points against synoptic experimental data, one might then be able to determine a source's size and the configuration of the scattering medium. One obstacle to this approach is the need to know both the velocity of the medium, and its turbulence profile along the line-of-sight. However, a rough knowledge of source size should be obtainable even without velocity information, given enough synoptic data, since the data should cluster about mean turbulence and velocity profiles. Also, day-to-day changes in the location of a traveling turbulent structure should be readily observable by monitoring the change in width of the spectrum on the same source each day, as the source size is then a constant and the velocity of the structure should also be nearly a constant.

Discussion - Experiment

We present in Figure B3 the slopes (α) and turnover frequencies (ν_3) for data taken during the months of June and July 1976 on the sources 3C48 and 3C273. The confidence in the estimate of α is generally lower than that for ν_3 due to the relatively lower confidence level of the high-frequency points as they approach the noise background level; therefore the following analysis relies more heavily on fitting ν_3 than on fitting α. The data in Figure B3 were taken from spectra obtained at 34.3 MHz with the University of Iowa COCOA-Cross radio telescope. Additional observations supplementing the COCOA-Cross data were taken at 38 MHz on the University of Maryland TPT radio telescope, also at Clark Lake Radio Observatory. It is immediately apparent that the data from the two sources lie in distinctly different areas of the (α, ν_3) plane. As the scattering regions in the interplanetary medium are physically separated for the two sources, and the sources have different angular diameters, this separation is not unexpected. The 3C48 points are sufficiently high in ν_3 that regardless of source size, we must assume (a) that the medium is almost always described as having a relative excess of turbulence near the earth (concentrated $\sim$ 0.1 AU in distance) or (b) that the assumed velocity of 400 km/sec is systematically exceeded in the medium. This is not true of the 3C273 points, which implies a difference in the character of the medium between the lines of sight to the two sources. In Figure B4, a subset of the data

from Figure B3 for which we obtained corresponding IPS velocity data from UCSD *(John Harmon, Private Communication)* is replotted, with the turnover frequency ν_3 corrected to a standard of V = 400 km/sec for all observations, e.g., $\nu_3(V) = \nu_3(400 \text{ km/s})\ (V/400)$. Included in Figure B4 are those ranges from Figure B2 which best fit each of the sources' points. Note that while the 7-13 slab ranges fit in ν_3, the α's calculated are much higher than those measured for angular diameters (θ) $\geq$ 1.0". It is clear that to a large degree the scatter of the data from the two sources in ν_3 in Figure B3 (replotted on Figure B4 for comparison in this format) is attributable to the differences in the velocities of the scattering medium along the lines of sight to the two sources.

For the period during which the observations overlap (day 182-day 204) the average velocity for 3C48 is nearly 200 km/sec higher than that for 3C273. The corotation delay between the two sources' scattering regions is nominally about 3 days during this 23 day overlap period (since their ecliptic longitude difference is $\sim 45°$) and the velocities for each source do not fluctuate by more than $\sim$ 100 km/sec (i.e., no one day weights the average significantly, nor does the velocity for 3C273 ever exceed that for 3C48) even though there were well-developed corotating streams observed at this time.

If one calculates the latitudes of the closest point of approach to the sun of the lines of sight to the two sources, the average gradient (assuming radial flow) over this 23 day period is > 20 km $s^{-1} deg^{-1}$.

There remains in Figure B4 a clear separation between the locus of the two sources' ν_3's. In general, the 3C273 points lie at lower cutoff frequencies than the 3C48 points. Part of this separation is due to a difference in the angular extent of the two sources. However, the points for 3C48 lie at higher turnover frequencies than can be explained by the model on the basis of a spherically symmetric interplanetary medium. Normally the distant medium would add power to the spectrum preferentially at low frequencies, which would result in low ($\sim$ 0.2 Hz) turnover frequencies. The higher frequency deviation of the 3C48 points may be due to two latitude effects. First, as the velocity data indicates, there is a strong latitudinal gradient in the solar wind velocity. As discussed earlier, the frequencies at which turbulence at a given distance along the line of

sight contributes to the observed spectrum are proportional to the bulk velocity of the turbulent region. *If* this velocity gradient *continues* to higher latitudes (> 10°), it could shift the fluctuation power contributed by the more distant medium (L > 1 AU) to higher frequencies; our computational model assumed a constant radial velocity. Second, the medium at ecliptic latitudes ≥ 10-15° may be less turbulent and/or have lower densities than the medium in the ecliptic. Low turbulence levels would produce less scattering, and if the higher latitudes have lower turbulence levels, then the turbulence level along the line of sight to a non-ecliptic source would decrease with distance as the latitude of the point along the line of sight increased. Because the distant medium contributes proportionately more power at low frequencies than the near-earth medium, the low turbulence levels in the distant medium would relatively reduce the low frequency power in the observed spectrum and ν_3 would increase. This would explain the apparent absence of power in the 3C48 spectrum at low frequencies.

There is another way of seeing that both of these effects contribute to the deviation of the 3C48 results from the spherically symmetric model. If we compare the distribution of the 3C48 points with the calculated ν_3's in Figure B2, we can see that they come closest to fitting the points for which the medium was modelled as extending only to the 13th of the twenty screens of equal scattering power. They are consistent with a source size of about ~ 0.5 to 3 arc seconds for q = 2.8. 3C273, on the other hand, is consistent with a source size of ~ 5 arc seconds, and a spherically symmetric medium. As its ecliptic latitude is 4°, its scattering region is essentially in the the sun's equatorial plane and the distribution of turbulence (and scattering) along the line of sight would be relatively insensitive to latitude dependence effects. Most of the 3C273 points lie at low turnover frequencies; however, they fall over a broad range of slopes ($1.3 \leq \alpha \leq 3.5$). The implication here is that the thickness of the scattering medium is varying, the higher slopes resulting from days on which the scattering was dominated by a relatively localized disturbance. Some of the range in α is also due to uncertainties in the estimate of the slope.

Modelling the electron density spectrum as a power-law with slope q, it was found that the best fits to the data (taken at 34.3 MHz) were obtained assuming q = 2.8 (rather than q = 3.6; q = 3.2 may also produce a good fit), with source sizes of ~ 0.5 to 3.0 arc-seconds for 3C48 and ~ 5.0 arc-seconds for 3C273. It was also found that the spectral turnovers for 3C48 lie at higher 3 dB frequencies than can be explained with a spherically symmetric medium. We interpret this to be the result of a latitudinal gradient in velocity, and when normalized by IPS velocity data, a continuation of that gradient in either turbulence, (with lower turbulence at higher latitudes) or in velocity (with higher velocities at higher latitudes) or both.

FIGURE CAPTIONS FOR APPENDIX B

FIGURE B1 Contribution to the scintillation index (band-passed from 0.1 to 1.5 Hz) as a function of distance along the line of sight for three source angular diameters (θ). The calculation was done for $F_o \propto r^{-4}$, q = 3.6, solar wind velocity V = 400 km/sec, and 34.3 MHz. The locations of the centers of slabs 7, 13, 19 and 20 are indicated.

FIGURE B2 (a) Numerically calculated ranges of ν_3. Each range is labelled according to source angular diameter, and they are grouped according to the choices of slabs to describe the medium. Variations in the medium profile are introduced within each choice of slabs by varying the elongation, resulting in a range of ν_3 rather than single points. Elongation was varied between 60° and 120°. The solar wind velocity was set at V = 400 km/sec, power law slope q = 2.8.
(b) Same as (a), for q = 3.6.

FIGURE B3 Data from June-July 1976 for 3C48 and 3C273 presented in the (α, ν) plane. Observations at 34 MHz from the University of Iowa COCOA-Cross radio telescope and at 38 MHz from the University of Maryland TPT radio telescope.

FIGURE B4 Subset of the data in Figure B3, adjusted to a velocoty V = 400 km/sec. Ranges of ν_3 from Figure B2 are selectively included for comparison with the data. The 3C48 points are consistent with a 0.5"-3.0" source with an absence of turbulence at latitudes > 10° (hence large distances, > 0.7 AU along the line of sight), and a 3.0"-7.0" source for 3C273 with a spherically symmetric medium. The best matches are for q = 2.8. The unadjusted ν_3's for each source are included for comparison. Note that before correction for velocity, the ν_3's for 3C48 are much more separated from those for 3C273, and that only three of the 3C48 points lie in the range of a spherically symmetric medium with V = 400 km s^{-1} while most of the 3C273 points lie in that range.

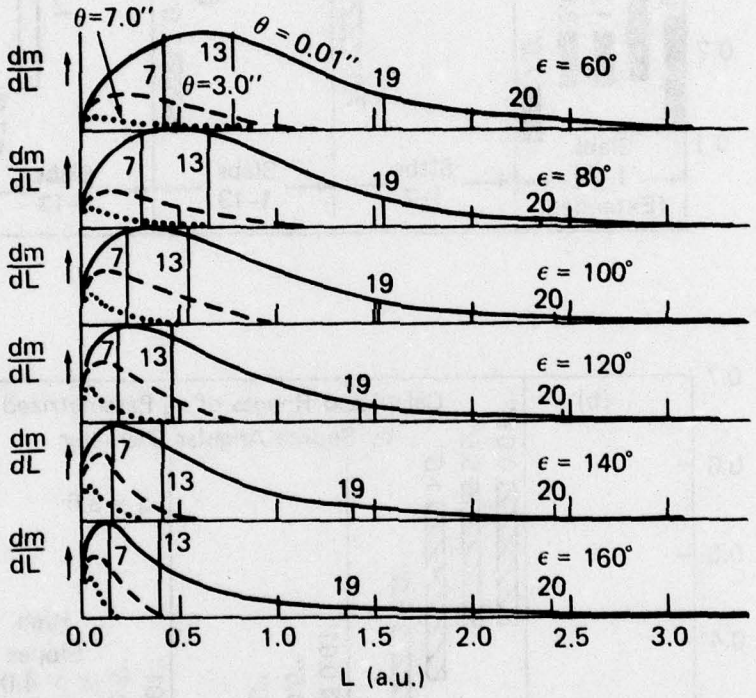
θ=7.0''
θ = 0.01''
θ=3.0''
7
13
19
20
ϵ = 60°
ϵ = 80°
ϵ = 100°
ϵ = 120°
ϵ = 140°
ϵ = 160°
dm/dL
0.0
0.5
1.0
1.5
2.0
2.5
3.0
L (a.u.)

FIGURE B1

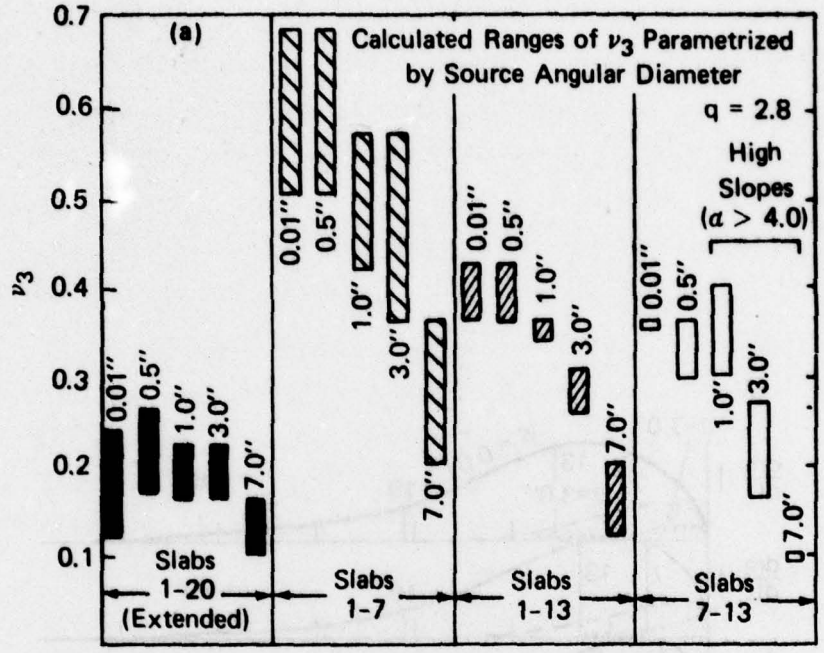
(a)
Calculated Ranges of ν_3 Parametrized by Source Angular Diameter
q = 2.8
High Slopes ($\alpha > 4.0$)
ν_3
0.7
0.6
0.5
0.4
0.3
0.2
0.1
0.01''
0.5''
1.0''
3.0''
7.0''
Slabs 1-20 (Extended)
Slabs 1-7
Slabs 1-13
Slabs 7-13

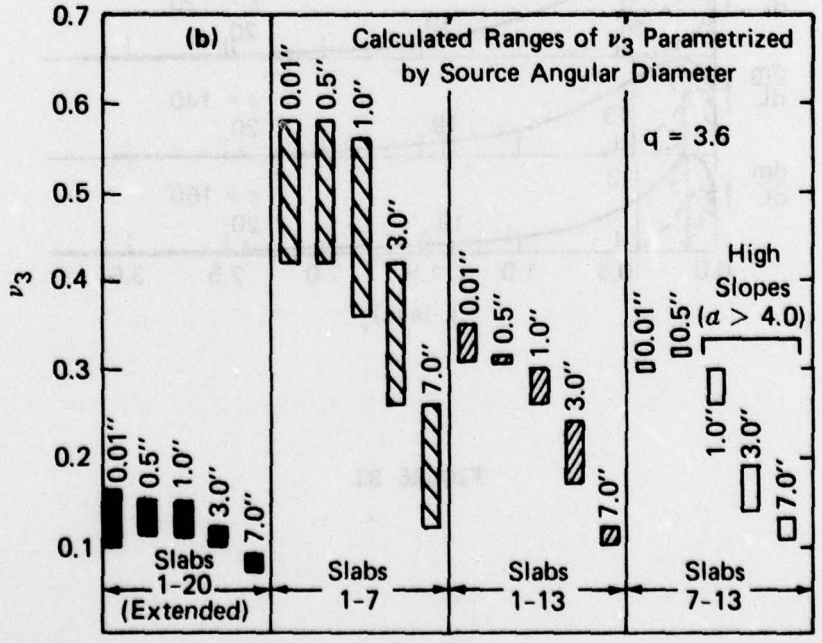
(b)
Calculated Ranges of ν_3 Parametrized by Source Angular Diameter
q = 3.6
High Slopes ($\alpha > 4.0$)
ν_3
0.7
0.6
0.5
0.4
0.3
0.2
0.1
0.01''
0.5''
1.0''
3.0''
7.0''
Slabs 1-20 (Extended)
Slabs 1-7
Slabs 1-13
Slabs 7-13

FIGURE B2

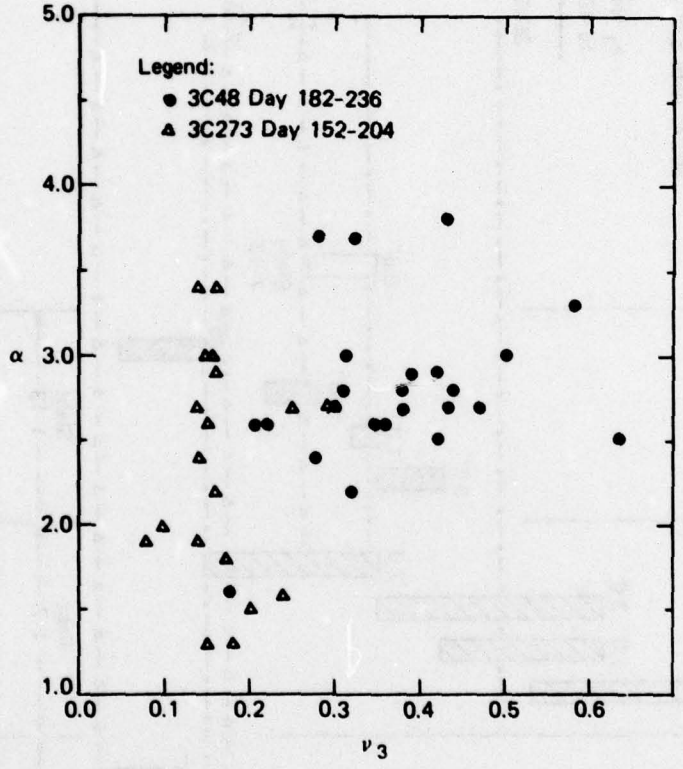
Legend:
3C48 Day 182-236
3C273 Day 152-204
5.0
4.0
3.0
2.0
1.0
α
0.0
0.1
0.2
0.3
0.4
0.5
0.6
ν_3

FIGURE B3

THE JOHNS HOPKINS UNIVERSITY
APPLIED PHYSICS LABORATORY
LAUREL, MARYLAND

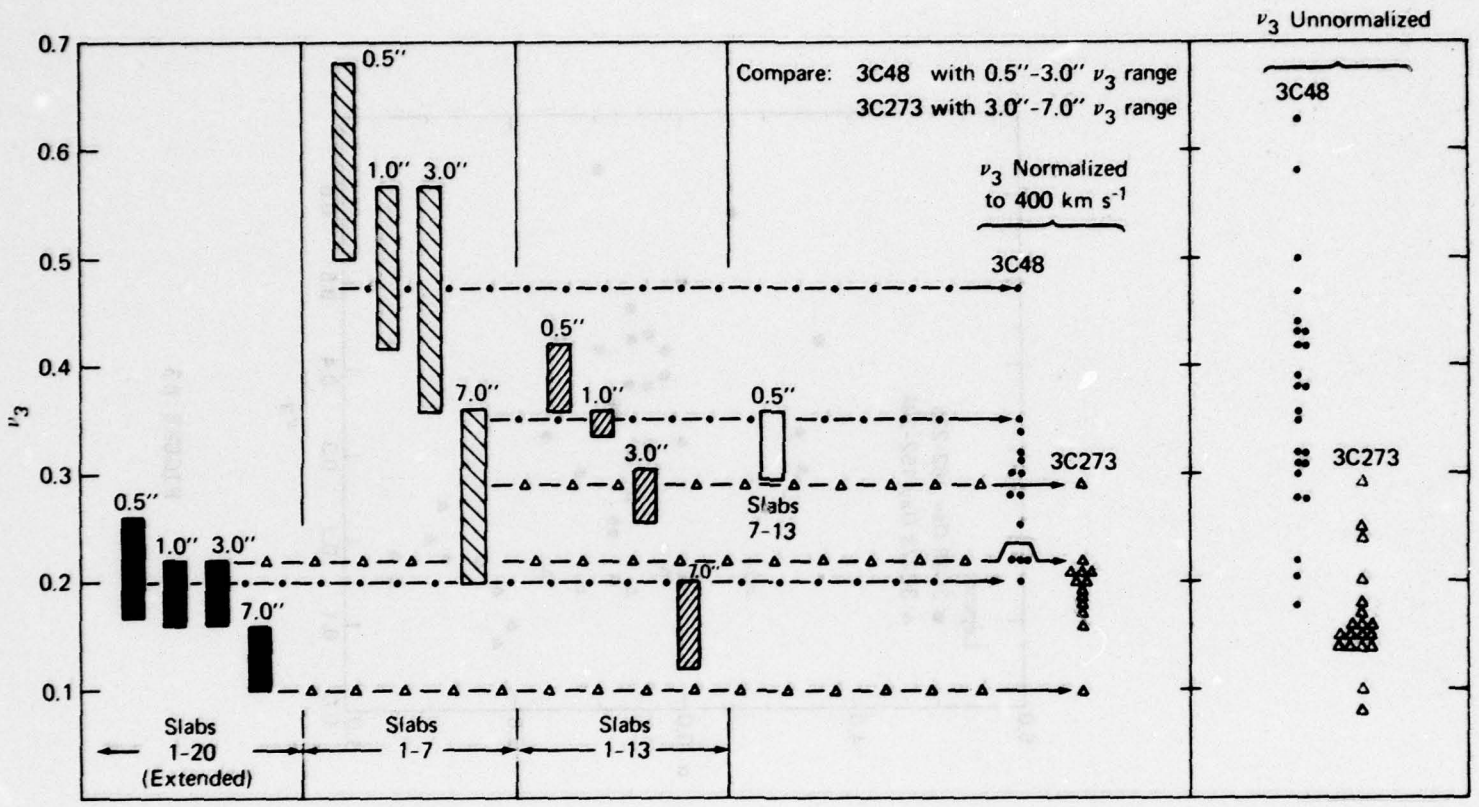

FIGURE B4

APPENDIX C

RAINFALL TOTALS

These rainfall records were all measured at the Anza-Borrego Desert State Park headquarters weather station located approximately 20 km from the Clark Lake Radio Observatory. Each month in which there was more than 1.5 inches of rain usually resulted in submersion of the dry lake bed under a few inches of water. Monthly totals of more than 3 inches resulted in flooding to a depth of more than 6 inches, and the August, 1977 rainfall resulted in flooding to a depth of more than 15 inches (Figure C1). Submersion of the d.c. control line cables for extended periods of time in the highly alkaline standing water resulted in rapid corrosion of the cables. Numerous short-circuits also developed, many occurring several months later as a result of water retention and continuing corrosion inside the multiconductor cable jacket. These problems compelled us to install a new, open wire, elevated d.c. control line feed system.

We will also note that in March, 1977, winds well in excess of 100 mph did extensive damage to the telescope. The subsequent repair and mechanical strengthening of the telescope makes it far more resistant to such winds in the future.

RAINFALL TOTALS BEGINNING 1962

	1962	1963	1964	1965	1966	1967	1968	1969	1970	1971	1972	1973	1974	1975	1976	1977	1978
January	1.11	0.10	0.47	0.05	0.49	0.24	—	2.39	—	0.23	—	0.48	3.38	0.05	0.20	1.13	4.44
February	1.55	0.89	0.23	0.07	0.12	—	0.04	0.97	0.53	0.11	—	1.17	—	0.30	3.14	0.07	1.82
March	0.32	0.78	1.19	0.04	0.46	—	0.59	0.37	1.38	0.07	—	0.80	0.39	0.28	0.73	1.14	2.79
April	—	0.54	0.10	0.83	—	0.59	0.81	0.05	0.36	—	0.05	—	—	1.01	0.27	—	0.22
May	—	—	0.13	—	—	—	0.04	0.35	—	0.19	—	—	0.23	0.02	0.22	0.05	
June	—	—	—	—	—	—	—	—	—	—	0.20	—	—	—	—	0.04	
Sub-Total	2.98	2.31	2.12	0.99	1.07	0.83	1.48	4.13	2.27	0.60	0.25	2.45	4.00	1.66	4.56	2.43	
July	—	—	0.03	0.58	1.26	0.14	0.57	0.06	0.31	—	0.03	—	0.30	0.56	0.17	—	
August	—	0.88	0.29	0.71	—	1.85	—	0.02	1.12	0.60	0.40	0.62	0.95	0.03	—	3.61	
September	—	1.38	0.19	—	0.03	0.28	—	0.35	—	0.19	—	—	0.04	1.53	4.40	—	
October	0.14	1.98	0.35	—	0.62	—	0.44	—	0.02	0.16	0.55	—	0.91	0.08	0.19	0.15	
November	—	0.30	1.16	3.29	0.83	0.82	0.03	1.25	0.58	—	1.56	0.18	—	1.08	0.22	—	
December	0.50	—	0.28	1.98	1.27	1.99	0.67	0.01	1.43	0.85	0.65	—	1.53	0.07	0.17	1.61	
Sub-Total	0.64	4.54	2.30	6.56	4.01	5.08	1.71	1.69	3.46	1.80	3.19	0.80	3.73	3.35	5.15	5.37	
TOTAL	3.62	6.85	4.42	7.55	5.08	5.91	3.19	5.82	5.73	2.40	3.44	3.25	7.73	5.01	9.71	7.80	

FISCAL YEAR TOTALS:

1962/1963	2.95	1967/1968	6.56	1972/1973	5.64
1963/1964	6.66	1968/1969	5.84	1973/1974	4.80
1964/1965	3.29	1969/1970	3.96	1974/1975	5.39
1965/1966	7.63	1970/1971	4.06	1975/1976	7.91
1966/1967	4.84	1971/1972	2.05	1976/1977	7.58

FIGURE CAPTION for APPENDIX C

FIGURE C1 Flooding of Clark Lake in August 1977. A local resident of Borrego Springs is canoeing in water more than 15 inches deep.

FIGURE C1